NRL Report 6591

Final Report on Gemini Experiment D-14 UHF-VHF Polarization Measurements

R. E. Ellis, J. W. Goodman, and W. Sievers

Aerospace Radar Branch
Radar Division

October 20, 1967

NAVAL RESEARCH LABORATORY
Washington, D.C.

This document has been approved for public release and sale; its distribution is unlimited.

CONTENTS

Abstract	ii
Problem Status	ii
Authorization	ii
INTRODUCTION	1
BACKGROUND	1
THEORY	2
EQUIPMENT	3
STATION INSTALLATION AND CALIBRATION	6
CONDUCTING THE EXPERIMENT	8
RESULTS	9
Prenoon Variation of the Ionospheric Electron Content Over Hawaii	9
Study of the Irregularities	16
Discussion of Errors	29
CONCLUSIONS	30
ACKNOWLEDGMENTS	30
APPENDIX — Derivation of the Faraday Effect for a Collision-Free Anisotropic Plasma	31

ABSTRACT

A vhf-uhf Faraday rotation experiment (D-14) was conducted in conjunction with six Gemini IX spacecraft transits over Kauai, Hawaii, and Antigua, British West Indies, on June 4, 1966. The rotational ambiguity at vhf was resolved by inspecting the received uhf polarization. The electron content and its inhomogeneities below the spacecraft have been determined. By comparing the results of the data analysis corresponding to four closely spaced transits of Gemini IX over Hawaii, a measure of the prenoon electron-content variation was obtained. Assuming a Chapman distribution and equilibrium conditions, the lower ionospheric temperature has been estimated to be approximately 1000°K at midday.

It has been found that the smaller ionospheric inhomogeneities (approximately 10 to 30 km) occur in greater numbers than would be anticipated strictly on the basis of their size and sample-time considerations. The irregularity excursion δC is found to be roughly an increasing function of irregularity scale δL, with the percentage excursion $P_{\delta c}$ increasing between 1% and 5% per 100 km.

PROBLEM STATUS

This is a final report on the problem. Unless otherwise notified, the problem will be considered closed 30 days after the issuance of this report.

AUTHORIZATION

NRL Problem R07-13
Project A37-538-006/6521/F019-02-01

Manuscript submitted May 12, 1967.

FINAL REPORT ON GEMINI EXPERIMENT D-14
UHF-VHF POLARIZATION MEASUREMENTS

INTRODUCTION

The purpose of this experiment was to measure the inhomogeneities in the electron content which exist along the orbital path of the spacecraft. Such measurements give increased insight into the structure of the lower ionosphere and its temporal variations.

This experiment was conducted by transmitting two cw signals from the spacecraft and receiving them at special receiving stations on the ground. Two separate receiving stations, one located at Kauai, Hawaii, and the other located at Antigua, British West Indies, were used to measure the amount of rotation, caused by the Faraday effect, that is introduced to the signals along their transmission path. The rotation angle was recorded, as a function of time, as the spacecraft passed over each of the two receiving stations. These rotation angles were entered into a computer program to calculate the electron content.

BACKGROUND

The concept of this experiment evolved from the ionospheric measurements being conducted by the Naval Research Laboratory employing the 150-ft-diam-dish radar system located at Randle Cliff, Md. These measurements involved radar signal returns from the moon as well as satellite signal transmissions.

The presence of free electrons in the ionosphere results in the fading of radio signals transversing all, or part of, the ionosphere. There are several types of fading, namely, absorption, scattering, and Faraday effect. At frequencies of 40 Mc/sec or lower radio signals can, under increased solar activity, be completely absorbed, resulting in a complete loss of signal. Scattering by the inhomogeneities in the electron distribution results in scintillation or rapid fluctuation of the signal level. The Faraday effect, which is the rotation of the plane of polarization of a linearly polarized radio wave in the presence of electrons in a magnetic field, may cause either regular or irregular fading, depending upon the state of the ionosphere.

An increased knowledge of the nature and origins of radio wave perturbation and the ability to predict its various forms is of fundamental importance to communication engineers and physicists. The size of the inhomogeneities causes irregular fading of radio waves. Also, the altitude dependence of the irregularities in electron distribution is of interest in a study of the origin of perturbations.

The electron content of the ionosphere will have a direct effect upon any radio signal originating in, received in, or passing through the ionosphere. An increased knowledge of the nature and perturbation of the electron content is, therefore, of military importance, since it will be directly related to the behavior of signals, communications, radar, etc., used in military operations.

Considerable work has been done to measure the irregularities in the electron distribution using several different approaches. One such approach involves radio astronomy techniques employing two antennas and suitable correlation analysis. In this

approach it is not possible to distinguish large irregularities with slow motion from small irregularities with rapid motion. Another approach uses signals from radio sources in the cosmos and signals or radar returns from superionospheric satellites. In any case this approach gives an integrated picture of ionospheric irregularities along the line of sight.

Much of the interest, from the military applications point of view, is concerned with the inhomogeneities in the lower regions of the ionosphere. Data from these lower regions are, however, rather sparse. The Gemini spacecraft orbited in the lower ionospheric region and moved rapidly; hence it was an ideal platform to give a rapid cross section of the region of interest.

THEORY

The theory embodied in the Faraday-effect method of determining the electron content of the ionosphere is relatively simple and has been used regularly in ionospheric investigations. The Faraday effect is the rotation of the plane of polarization of a linearly polarized radio wave. The rotation of the electric vector of the radio wave is directly proportional to the electron content along the path of propagation and the component of the earth's magnetic field parallel to the path and is inversely proportional to the square of the radio frequency.

Under conditions of quasi-longitudinal propagation and at frequencies above 100 Mc/sec, where the plasma frequency and the gyro frequency are relatively small, the Faraday rotation is given by the approximate formula

$$\Omega = 2.97 \times 10^{-2} f^{-2} \int_0^S (H \cos \theta) N \, ds , \tag{1}$$

where

Ω is the rotation angle in radians,

f is the radio frequency in cycles per second,

H is the total magnetic field intensity in ampere-turns per meter,

θ is the angle between the ray path and the magnetic field vector,

N is the electron density in electrons per cubic meter,

s is the distance measured along the ray path in meters, and

S is the distance from the ground antenna to the spacecraft in meters.

The derivation of Eq. (1) is given in the Appendix. The equation is valid strictly for radio frequencies in excess of 100 Mc/sec. Below 100 Mc/sec higher-order terms, which are neglected in this treatment, become increasingly important. Also, at frequencies below 100 Mc/sec and at low elevation angles, severe refraction and path-splitting effects may introduce additional complications.

The Faraday rotation may, at the lower frequencies, exceed a complete revolution, resulting in an $n\pi$ ambiguity. One method of removing this ambiguity is to use two frequencies, one at vhf and the other at uhf, with one frequency high enough so that the total rotation angle cannot be ambiguous. For this experiment, using a spacecraft altitude of

160 naut mi, the rotation angle should always be less than 180° at a frequency of about 400 Mc/sec. By using a second frequency in the 100 Mc/sec range accurate measurements, without ambiguity, can be made.

The selection of the exact radio frequencies was influenced by several factors in addition to frequency spectrum availability. The first factor, the variations in the predicted subsatellite electron content, is a function of sunspot activity, solar zenith angle, and the spacecraft altitude. The second factor, the variations in the effective magnetic field parameter, is a function of the field station location and the spacecraft orbital paths. The third factor, the total angular orientation error, is a function of spacecraft antenna orientation, the purity of polarization of the transmitted signals, and the measurement errors. The first two factors can be adequately estimated, but the third factor is the more difficult one to assess.

EQUIPMENT

The equipment used for this experiment is divided into two categories: equipment located in the spacecraft and equipment located on the ground.

A block diagram of the system mounted in the spacecraft is shown in Fig. 1. This system consists of a dual-frequency transmitter, a diplexer, and a colinear dipole antenna mounted on an extendable boom. The dual-frequency transmitter* generates two cw signals at frequencies of 133.9 Mc/sec and 401.7 Mc/sec. These two frequencies are combined in the diplexer so that both frequencies can be fed over a single coaxial cable

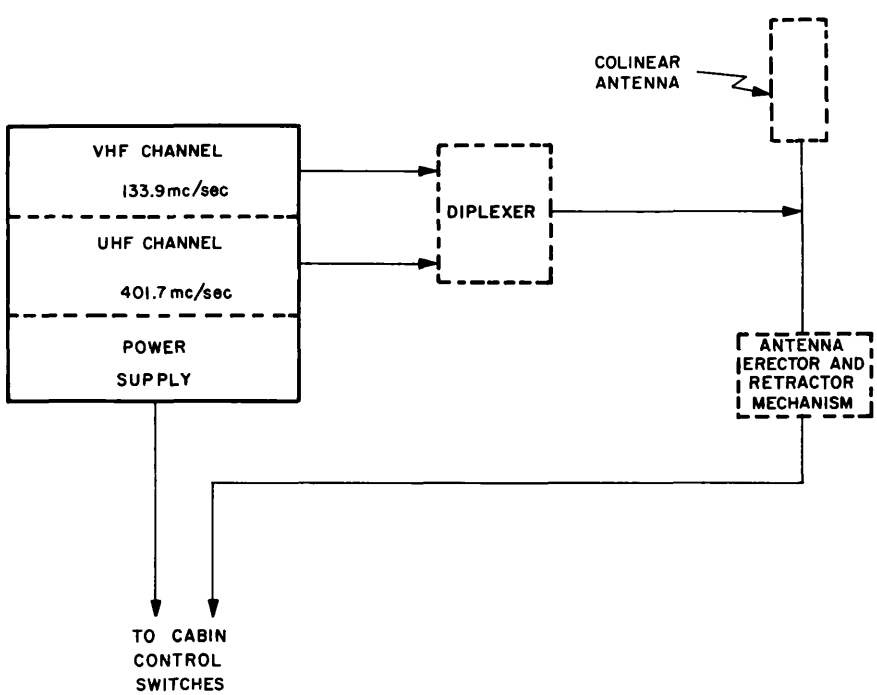

Fig. 1 - Transmitter system

*A.E. Leef, "A Dual Channel VHF-UHF Transmitter for Gemini Experiment D-14," NRL Report 6484, Jan. 23, 1967.

to the antenna. The colinear dipole antenna* is designed to radiate efficiently at both frequencies. A boom mount is used so that the antenna can be contained entirely inside the spacecraft prior to and during the launch and then deployed and positioned about 8 ft from the skin of the spacecraft after the spacecraft is in orbit.

A block diagram of the ground receiving station is shown in Fig. 2, and a composite photograph of the station equipment, less the antenna, is shown in Fig. 3. A photograph of the antenna installation at Antigua, B.W.I., is shown in Fig. 4.

The receiving antenna is a 28-ft-diam parabolic dish with a special cross-dipole feed system to separate the two signals received from the spacecraft transmission into their vertical and horizontal components. During any spacecraft pass over a ground

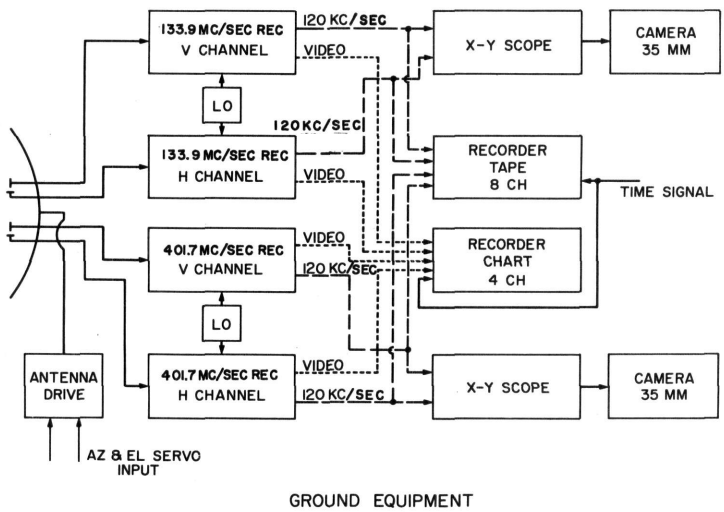

Fig. 2 - Receiving system

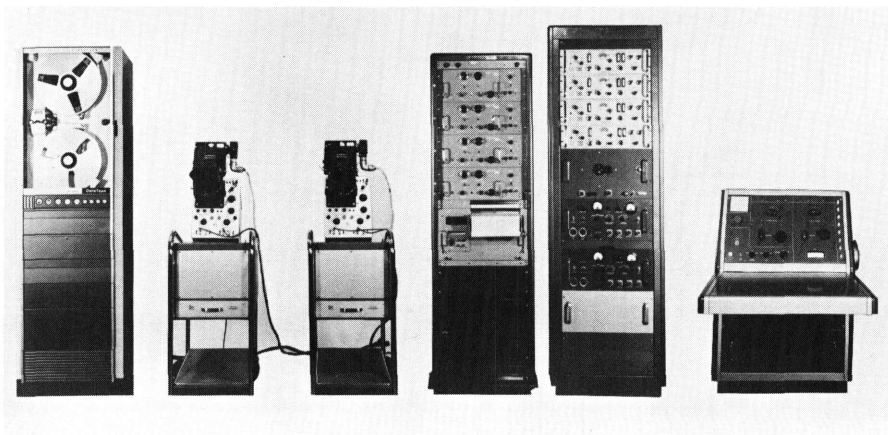

Fig. 3 - Composite photograph of the ground receiving system

*R.L. Eilbert, "Antennas For The Gemini VHF-UHF Polarization Experiment (D-14)," NRL Report 6501, Mar. 2, 1967.

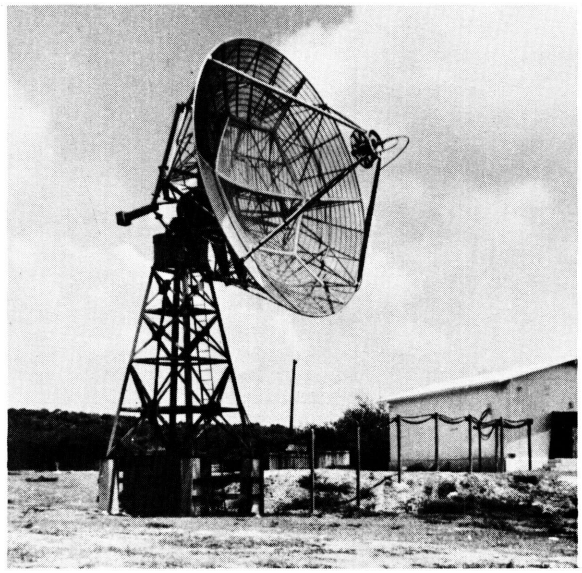

Fig. 4 - Receiving antenna at Antigua, B.W.I.

receiving station, when the experiment is conducted, the receiving antenna will be slaved from a nearby tracking radar so that it points at or tracks the spacecraft as it passes the receiving station. As the two cw signals are received from the spacecraft transmission, the antenna-feed separates each signal into its vertical and horizontal components. The vertical components of each frequency are fed down a single coaxial line to a special frequency-separating filter. The filter has two outputs; one is the vertical component of the 133.9-Mc/sec signal, and the other is the vertical component of the 401.7-Mc/sec signal. The horizontal components of the two frequencies are fed down a second coaxial line to another separating filter, to provide the 133.9-Mc/sec and the 401.7-Mc/sec horizontal components.

The vertical and horizontal components of the 133.9-Mc/sec signal are fed through ganged step attenuators into the two inputs of the 133.9-Mc/sec dual-channel receiver, and the vertical and horizontal components of the 401.7-Mc/sec signal are fed into the two inputs of the 401.7-Mc/sec dual-channel receiver. In each dual-channel receiver the signal components are heterodyned down from their rf to a frequency of 120 kc/sec. Common local oscillators are employed in each of the dual-channel receivers to eliminate oscillator-introduced phase errors so that, insofar as possible, identical phase characteristics can be maintained in the two channels. The 120 kc/sec signals from the 133.9 Mc/sec receiver are fed into one x-y scope, and the 120 kc/sec signals from the 401.7-Mc/sec receiver are fed into a second x-y scope. In each case the horizontal component of the signal was fed into the horizontal amplifier of the x-y scope, and the vertical component of the signal was fed into the vertical amplifier of the x-y scope. In this manner the Faraday rotation angle of each signal was reproduced and displayed. For example, if the rotation angle were 45° both the vertical and horizontal outputs from a receiver would have equal amplitudes and phase, and a 45° line would be traced on the face of the scope. If the Faraday rotation angle had been 135°, then the receiver outputs would have been equal but out of phase, and a line 135° from zero would be displayed on the scope. The two x-y scope displays were photographed with a 35-mm frame-by-frame camera at approximately 2-1/2 frames per second. On each photo frame, in addition to the Faraday rotation angle, clocktime and rf attenuator settings were recorded. Photographs of the scope display of the Faraday rotation are shown in Figs. 5 and 6.

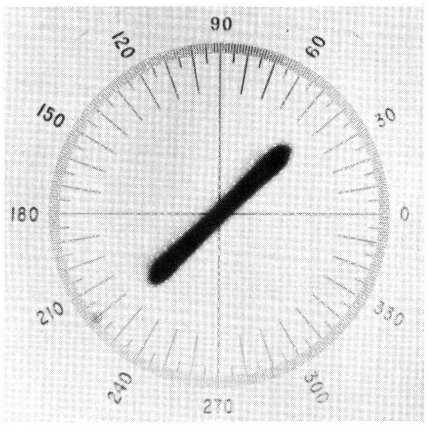

Fig. 5 - x-y scope display of the rotation angle

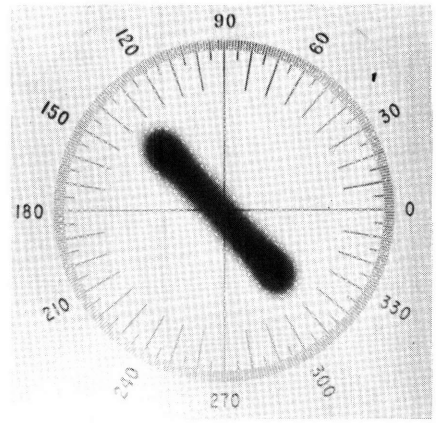

Fig. 6 - x-y scope display of the rotation angle

When the 120-kc/sec signals from the two receivers are displayed on the x-y scopes, they are also recorded on magnetic tape. In this manner a record of the 120-kc/sec signals is maintained, and the x-y scope displays can, if desired, be reproduced later, whenever necessary. With the 120-kc/sec signals, time reference signals and rf attenuator-setting signal tones are also recorded on the magnetic tape. Therefore, all the information necessary for data reduction that is available from the receiving station is available on the magnetic tape record.

The 120-kc/sec rf signals in each of the receivers are detected, and their envelopes are fed to and recorded on a paper-chart recorder. These recordings can be examined later, and information concerning the perturbation in electron content along the spacecraft path can be extracted from the short time fluctuation in the envelopes. In addition, the chart recordings provided a visual monitor of the signal levels; hence, when necessary, the proper rf attenuation could be manually inserted into the receiver input lines. Time was recorded directly on the charts by the recorder, but the attenuator settings had to be entered manually.

STATION INSTALLATION AND CALIBRATION

Two ground station installations were made, one at Kauai, Hawaii, and the other at Antigua, B.W.I. In general, the installation of the systems at both sites was the same. The calibration phase of each installation consisted of zeroing the elevation and azimuth synchro system, adjusting the transmission lines to eliminate or minimize phase error, and balancing channel gains at each frequency. Because of different situations at each ground station site the technique for the synchro system zero was slightly different at the two sites.

At Antigua two bore-site locations were used: one to align the horizontal servo system in the antenna, the other to align the elevation servo system. An FPQ-6 tracking radar would be the system supplying tracking signals from which the experiment antenna would be slaved. The antenna of this system was associated with an optical bore-sight system having a remote TV display. This optical system, along with a dipole antenna mounted at the base of the FPQ-6 antenna, was used to zero the horizontal servo system for the D-14 antenna.

The FPQ-6 optical system had sufficient resolution to enable pointing its antenna at the center of the azimuth axis of the D-14 antenna pedestal. When the antenna was pointed 180° from this azimuth position, slave signals were generated which directed the D-14 antenna toward the FPQ-6 antenna. A 401.7-Mc/sec cw signal was radiated from the boresight dipole antenna, located at the base of the FPQ-6 antenna pedestal, and was received at the D-14 antenna. With the FPQ-6 azimuth slaving signals controlling the azimuth position of the D-14 antenna, the servo system in the D-14 system was adjusted to point the D-14 antenna at the dipole antenna, or, in other words, at the FPQ-6 antenna. The center of the D-14 antenna beam was determined by locating the 1-dB-down points on either side of the maximum output from one of the 401.7-Mc/sec receiver channels and assigning a point midway between the 1-dB-down point as the center of the beam. After the azimuth synchro system was adjusted the indicating dial servo system was adjusted to indicate the correct azimuth position.

A platform on a Navy Station sleeve antenna was used to bore-site the elevation of the D-14 antenna. An official survey of the receiving station revealed that the top of the railing on the Navy antenna platform was 0.85 ft above a plane through the elevation axis of the D-14 antenna. On the basis of this information it was possible to place a transit on the platform in such a position that the center of the transit barrel, in a level position, was in the same plane as the center of the antenna elevation axis. Under this condition, with a zero elevation signal from the FPQ-6 radar and the D-14 antenna looking at the transit, the elevation servo system was adjusted to zero by observing, through the transit, that the antenna-feed was in the same plane as the center of the antenna dish. The antenna was so constructed that an assembly joint was in the same plane as the center of the dish and the elevation axis. This joint was used as a reference, when looking through the transit, to locate the antenna-feed in the same plane as the center of the dish. When this adjustment was completed the elevation dials were adjusted to indicate zero degrees elevation.

At the receiving station on Kauai a single bore-site tower was used to calibrate the D-14 antenna servo system. The elevation and azimuth angles between the D-14 antenna and a convenient spot near the top of this tower were determined by an official survey. The same general technique, using a transit on the bore-site tower, as employed at Antigua was used to adjust the antenna servo system. This installation was also checked by radiating from a dipole antenna on the bore-site tower.

The gain and phase balance of the receiving systems were adjusted in the same way at both sites. The gain of each of the dual-channel receivers was adjusted by feeding equal signal levels, at the appropriate frequency accurately set by a counter, into each of the receiver inputs. By using a single signal generator and splitting the power the display on the x-y scope would be a line at an angle of 45° from the horizontal. An unbalance in gain would be indicated by a deviation from 45° on the x-y display and would be corrected by an adjustment of the gain of one of the receiver channels. This gain balance was checked and adjusted, if necessary, just prior to each experiment period.

The adjustment of system phase was necessary to compensate for the slight differences in coaxial cable length — which are inevitable despite all efforts to maintain equal lengths — between the antenna-feed and the receiver inputs. Any phase unbalance between the two channels of a receiver, from antenna to receiver output, was indicated by the display of an ellipse on the x-y scopes, instead of the desired straight-line display. The dipole antenna oriented at 135° was used to radiate the appropriate frequency from the bore-site tower. The D-14 antenna was pointed directly at the dipole antenna, which was energized by a signal generator, and the signal received was displayed on the x-y scope associated with the particular frequency radiated, either 133.9 Mc/sec or 401.7 Mc/sec. To insure that the radiated signal and the receiver rf output were at the proper frequency they were both checked and monitored by frequency counters. The system installation included a line stretcher in one coaxial line of both pairs of coaxial lines, one pair for

each frequency. By adjusting the line stretcher in the 133.9-Mc/sec line, the x-y display was adjusted to be a line, oriented at 135°. This adjustment of phase was made for both the 133.9-Mc/sec and 401.7-Mc/sec receivers.

The overall sensitivity of each of the receiving stations was also checked using the bore-site tower and a dipole antenna. At both sites the distance between the D-14 antenna and the bore-site tower was accurately known from the official site survey. A known power level, 1 mW, was transmitted from the dipole antenna on the bore-site tower, and the received signal-to-noise ratio (S/N) was measured. This S/N was compared to the S/N that was calculated for this power transmittal, range, and other system parameters and losses. The measured and calculated values of the S/N at both sites were in agreement within several dB, indicating that the overall system sensitivities were satisfactory.

CONDUCTING THE EXPERIMENT

This experiment was scheduled to be flown on the Gemini spacecrafts Nos. 8 and 9 (GT-8 and GT-9). The procedure for operating the equipment in the spacecraft was quite simple and required a minimum of effort by the astronauts. After the spacecraft was placed in orbit, and prior to conducting the experiment, the astronauts were required to extend the colinear dipole antenna. This was accomplished by placing the antenna control switch in the "extend" position, which energized the boom extension motor and caused the boom to extend. During the orbits in which the experiment was conducted the astronauts were required to turn on the dual-frequency transmitter about two minutes prior to reaching the radio horizon of the receiving site. The operation of turning on the transmitter involved only the positioning of the transmitter control switch to the "on" position. The primary effort by the astronauts involved placing and maintaining the attitude of the spacecraft such that the colinear dipole antenna always pointed to the center of the earth. From a zero, zero-zero attitude this maneuver required about a 158° roll to the right, a 17° nose-down pitch, and a 90° yaw to place the nose or small end of the spacecraft away from the ground station. The 90° yaw maneuver was required, because the direct-to-cross polarization antenna patterns of the antenna were considerably better when viewed from the back or large end of the spacecraft. This attitude had to be maintained throughout the flight over the ground station. After the spacecraft passed beyond the radio horizon of the ground station the transmitter was turned off, and any spacecraft attitude could be assumed.

The experiment was never conducted with GT-8 because the flight terminated early. The following discussion will be concerned only with GT-9 as it was planned and actually flown.

The integration of the operational procedures into the flight plan was concerned primarily with the method of controlling the spacecraft attitude. Three modes, A, B, and C, of spacecraft control were detailed and written into the procedures. Mode A involved the use of the stable platform and the computer; hence, it was the most accurate mode and the one that would be preferred even though it required the highest power consumption. Mode B was the next most desirable mode, since it also involved the use of the platform, but not the computer. Pitch and yaw were to be maintained by reference to the "8-ball." The least desirable operating mode, Mode C, did not involve the use of either the platform or the computer. Attitude would be maintained by use of a reticle mounted on the window and referenced to the horizon.

One other problem in integrating the operational procedure into the flight plan involved the antenna. Since the small-diameter end of the antenna is folded and is spring loaded to deploy the first time it is extended, it cannot be automatically refolded. When the antenna boom is retracted, after being extended the first time, about 26 in. of the small-diameter portion of the antenna will remain beyond the surface of the spacecraft.

In addition to presenting a possible extravehicular activity (EVA) hazard under such conditions the antenna is also subject to being bent. A bent antenna would destroy the necessary linear polarization; hence, it would negate the experiment. Because of these factors it was decided not to deploy the antenna until after the EVA was completed.

The only problem encountered in integrating the experiment into the mission plan concerned the number of times the experiment was to be conducted. Since the experiment is statistical in nature, the more data the better, and no data were obtained from the flight of GT-8, a minimum of ten experiment operations over each of the two ground stations was requested. Because of other mission operations only four operations over each of the ground stations was scheduled in the final flight plan. This plan called for conducting the experiment during orbits 26, 27, 30, and 42 over the Antigua station and during orbits 30, 32, 33, and 34 over the Hawaii station.

The astronauts were given a formal briefing covering the objectives of the experiment, anticipated procedures, and problems. Since the operational procedures for this experiment were quite simple, it was concluded that no special training would be required. The astronauts believed that any training to maintain spacecraft attitude would be more than adequately covered by the normal flight-simulator training.

There were no deviations from the planned operational procedure for the experiment, insofar as the operation of the experiment equipment was involved. As far as the mission was concerned the experiment operations did not follow the planned mission. The reason for this deviation was that the entire mission was modified following the first rendezvous operation.

Because of the change in mission plan, this experiment was conducted prior to the EVA operation. Six experimental operations were made, one over Antigua during orbit 18 and five over Hawaii during orbits 17, 18, 19, 20, and 21.

Three more operations were scheduled over the Hawaii station during orbits 34, 35, and 36, but the experiment antenna was damaged when the astronaut drifted into it during EVA. The antenna broke rather than bent, which is surprising since this member of the antenna was constructed of 6061T6 aluminum alloy — ordinarily one of the most ductile aluminum alloys.

During all the experiments the signals received at both ground receiving stations were about 30 dB lower than had been planned. Calibration tests of both ground stations, using the bore-site towers, indicated that the system sensitivity was normal. This, therefore, placed the problem with the equipment in the spacecraft. Unfortunately, there was no telemetry to monitor the equipment, and all the equipment was located in the adapter sections and not recoverable. As a result, it is possible only to speculate concerning the location of the malfunction.

Fortunately, the experiment was designed to produce signal-to-noise ratios at the receiver outputs of about 50 dB. Even with the signal levels reduced by about 30 dB the signal levels received were sufficient to produce quite usable results. The primary effect of the lower signal levels was to reduce, somewhat, the accuracy of the end results.

RESULTS

Prenoon Variation of the Ionospheric Electron Content Over Hawaii

Because the Hawaii transits of the Gemini IV spacecraft, for which experiment D-14 was conducted, were only spread over a fraction of a single day, it was impossible to

deduce the diurnal variation of the subsatellite electron content. This, of course, was anticipated. Indeed, the primary purpose of D-14 was not to determine the mean content (integrated electron density) – rather it was to determine the inhomogeneities associated with the mean content. Nevertheless, by computing the mean content corresponding to each D-14 Gemini IV transit over Hawaii, a measure of the variation in electron content between 0700 and 1300 Hawaii Standard Time (HST) was obtained.

The first step in the data analysis was to resolve the vhf polarization ambiguity. This ambiguity was easily resolved, since the ratio of the polarized rotation at 401 Mc/sec to the rotation at 133 Mc/sec is known (the ratio is 1:9, theoretically) and the rotation at 401 Mc/sec is not ambiguous for lower ionospheric propagation paths. The amount of Faraday rotation between the spacecraft (at an altitude of 300 km) and the receiving station is given by the equation

$$\Omega = 2.97 \times 10^{-2} f^{-2} \bar{\psi} \int_0^{300} N\,dh\,, \tag{2}$$

where $\bar{\psi}$ is the mean magnetic field parameter (amp-turns/m), f is the radio frequency (cycles/sec), the integral is the subsatellite content (electrons/m^2), and Ω is the Faraday rotation (radians). Taking 100 km to be an upper limit for some effective slab thickness τ such that

$$\int_0^{300} N\,dh \approx 1.24 \times 10^{10} f_p^{\,2} \tau\,, \tag{3}$$

where f_p is the maximum plasma frequency below the spacecraft, we may estimate Ω quite easily.

Taking $\bar{\psi}$ to be 40 amp-turns/m, f_p to be 10 Mc/sec, and f to be 401 Mc/sec, Ω is less than 1 radian. Typically, however, there exists a region during the transit of the spacecraft such that $\bar{\psi}$ is considerably less than the assumed value. Hence, the resolution of the uhf polarization angle is surely no problem for at least some small fraction of time during the transit, and it follows that the vhf polarization ambiguity problem is solved.

Subsequent to resolving the vhf polarization ambiguity, values of the subsatellite electron content were computed by means of the formula

$$\int_0^{300} N\,dh = 1.04 \times 10^{16}\ \Omega/\bar{\psi}\ (133\ \text{Mc/sec})\,, \tag{4}$$

where Ω is in degrees and will be throughout the remainder of the report. The values of

$$\int_0^{300} N\,dh\,,$$

which are more or less representative of each transit for which the D-14 experiment was conducted, are given in Table 1. For H18, H19, H21, and A18,* the tabulation corresponds to a transit average. Due to the small amount of rotation exhibited throughout the data corresponding to H20 and because of the relatively poor tracking on H17, a single

*Hawaii transits are denoted by the abbreviation H, and the Antigua transit is denoted by A. The transit numbers are affixed.

Table 1
Average Ionospheric Electron Content Over Hawaii and Antigua

Location	Transit	Time	Content (m^{-3})
Hawaii	17	06:41:07*	4.91×10^{16}
Hawaii	18	08:15:15	7.63×10^{16}
Hawaii	19	09:49:45	7.81×10^{16}
Hawaii	20	11:26:00†	7.87×10^{16}
Hawaii	21	13:01:30	6.47×10^{16}
Antigua	18	07:02:30	7.68×10^{16}

*Single point determination due to poor tracking on the ascending portion of the track.
†Single point determination at the closest point of approach.

value of content is presented in Table 1 for each of these two transits. To guarantee the optimum precision maximum rotation was the criterion used for the single-value selection. The Hawaii values are presented in Fig. 7 along with the F1 and F2 maximum electron densities. By applying Shimazaki's approximation the height of the F2 maximum may be estimated, and the results appear in Fig. 8 for the period between 0600 HST and 1300 HST over Maui, Hawaii. It is evident from Fig. 7 that

$$\int_0^{300} N\,dh$$

should be an increasing function of time, and this is in general agreement with the computed results. The value of

$$\int_0^{300} N\,dh$$

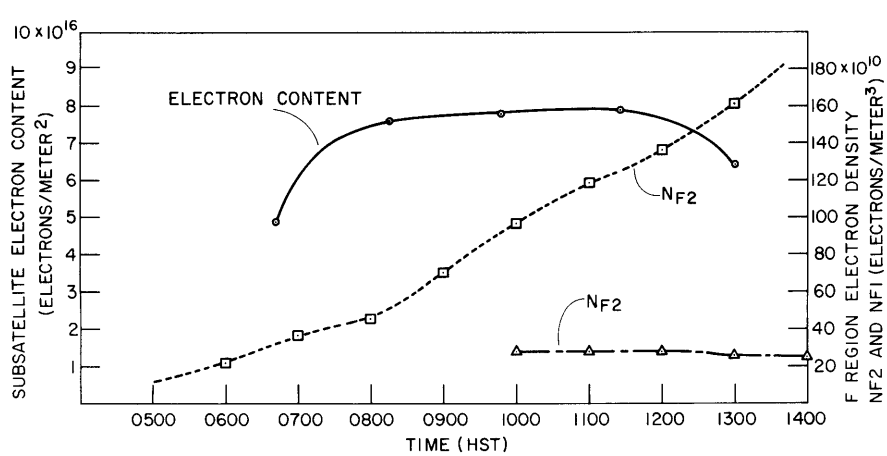

Fig. 7 - Subsatellite electron content over Hawaii on June 4

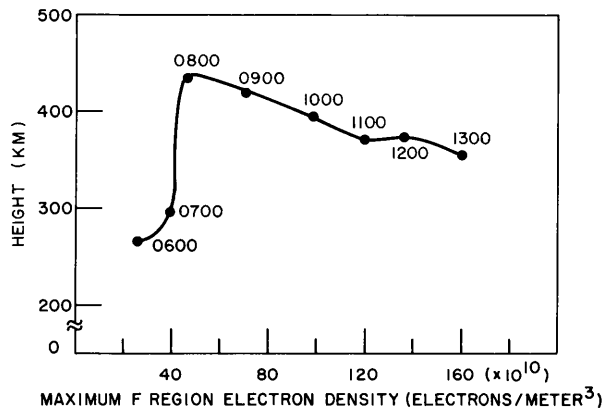

Fig. 8 - F2 maximum electron density and altitude over Maui, Hawaii, on June 4, 1966, as suggested by ionosonde data (specifically values of M(3000)F2 and foF2). The altitudes of the F2 maximum was deduced from Shimazaki's formula: hF2 = [1490/M(3000) F2] - 176; the maximum density was deduced from the relation NF2 = 1.24×10^{10} $(\text{foF2})^2$ where foF2 is in Mc/sec and NF2 is in electrons/m^3.

associated with H21 is an exceptional case, since the integral decreases by 17% between H20 and H21, contrary to the anticipated increase based upon any simplified constructions.

If the quantity

$$\int_{250}^{300} N\,dh$$

increases more rapidly than does

$$\int_{0}^{250} N\,dh,$$

an effective decrease in the ionospheric slab thickness results. As a result the height of the ionospheric mean $\bar{h}$ (for that portion of the ionosphere below the satellite, $h_s \cong 300$ km) will have a tendency to approach 300 km. Since ψ is a decreasing function of altitude, it follows that the error in $\bar{\psi}$ (for $\bar{h}$ = 250 km, for example) which occurs from the neglect of this effect, will be positive. Therefore, we must subtract some increment $\delta\bar{\psi}$ from $\bar{\psi}$ to compensate, and this will necessarily magnify the computed value of the content

$$\int_{100}^{300} N\,dh$$

to some extent.* However, even if $\bar{h}$ were to progress from 250 km to 300 km (physically unrealistic) the ratio of $\delta\bar{\psi}$ to ψ represents only an error of a few percent. It is apparent

*Since $\int_{0}^{100} N\,dh \ll \int_{100}^{300} N\,dh$, it follows that $\int_{0}^{300} N\,dh \approx \int_{100}^{300} N\,dh$.

that the inappropriate selection of the ionospheric mean height $\bar{h}$ cannot account for a 17% reduction in content, and we are forced to conclude that the reduction in

$$\int_{100}^{300} N\,dh$$

between H20 and H21 is real. This situation could be explained by the presence of an extensive upward drift, which above 220 km, for example, is a decreasing function of altitude. The net effect would be a severe depletion of electrons below 220 km and an accumulation between 220 km and the spacecraft altitude. If the total content had been invariant, we would require that the upward drift rate vanish at the spacecraft; however, since the content

$$\int_{100}^{300} N\,dh$$

is diminished between H20 and H21, a net loss of 1.40×10^{16} electrons/m^2 occurs as a result of upward drift under equilibrium condition. (Equilibrium implies that electron production is balanced by electron decay throughout the ionosphere.) Consequently, the time rate of change of the loss of electrons through a square-meter surface at 300 km is approximately 10^{16} electrons/hr. The mechanism responsible for this phenomenon will not be discussed here, but it is possible that electromagnetic forces play an important role. ($\boldsymbol{E} \times \boldsymbol{H}$ drift near the magnetic equator would be directed vertically if there were a significant horizontal electric field present in the lower ionosphere.)

Recently, Ross* has determined values of the electron content over Huancayo, Peru, for July and August 1962. His measurements were made at 54 Mc/sec and represented the total ionospheric electron content, since the transmitting satellite (1961 Omicron I) was orbiting at an altitude of 1000 km. After having normalized his values to a fixed value of solar flux (S = 100 at 10.7 cm) Ross depicts a midday peak in content of between 2 and 3×10^{17} electrons/m^2. Assuming that the ionosphere is Chapman-distributed,† it may be shown that the ratio of

$$\int_0^{\infty} N\,dh \text{ to } \int_0^{300} N\,dh$$

is 3.15, provided that the peak electron density corresponds to an altitude of 300 km.‡ It has been shown experimentally that the ratio is generally much larger at night.§ but

*W.J. Ross, J. Geophys. Res. 71(No. 15):3671 (Aug. 1, 1966).

†The Chapman profile depends on the validity of a number of simplifying assumptions: (a) monochromatic radiation, (b) isothermal atmosphere, (c) constant force of gravity with altitude, (d) uniform composition of atmosphere, and (e) exponential decrease of atmospheric density with height, but a conventional representation. It may be written as

$$Ch(\delta h) = \exp\left[\frac{1 - \left(\frac{\delta h}{H_s}\right) - \exp\left(\frac{-\delta h}{H_s}\right)}{2}\right],$$

where $\delta h = h - hF2$ is the distance from the $F2$ maximum and H_s is the scale height of the distribution. Physically $H_s = kT/mg$, where k is Boltzmann's constant, g is the gravitational acceleration, and T and m are the temperature and mean molecular mass, respectively. The distribution may be denormalized by multiplying $Ch(\delta h)$ by the $F2$ maximum electron density. Figure 9 illustrates the Chapman profile for H_s equaling 50 km to 120 km.

‡J.M. Goodman, "Prediction of Faraday Rotation Angles at VHF and UHF," NRL Report 6234, Apr. 28, 1965.

§G.H. Millman, J. Geophys. Res. 69(No. 3):429 (Feb. 1, 1964).

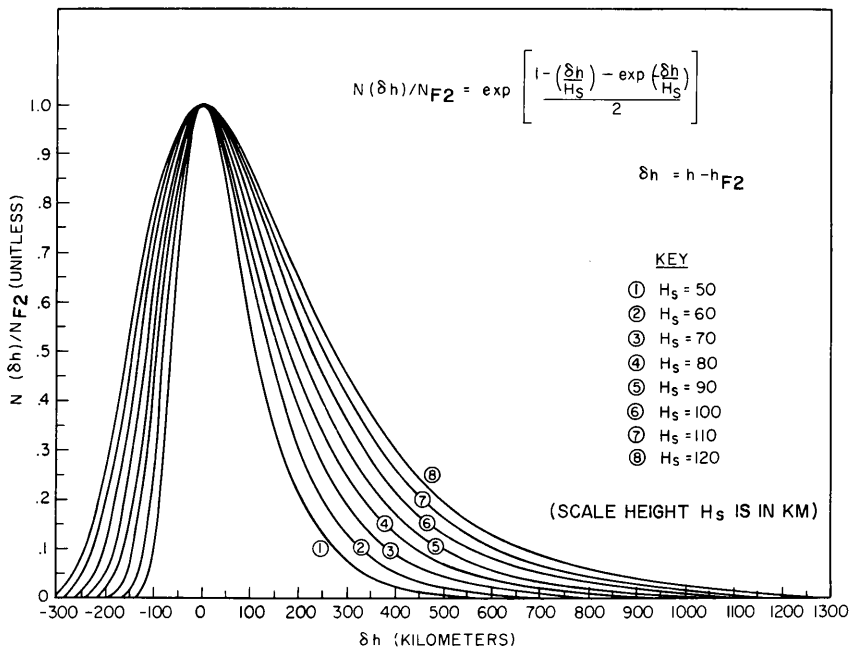

Fig. 9 - Normalized Chapman distributions of electrons as a function of altitude

possibly smaller during the day;* considering that the approximations are rough, that $h_s \approx 300$ km, and that the ionosphere is of the simple Chapman form, it follows that the Gemini IX results are in essential agreement with the data published by Ross and other workers. Radar returns from the Echo II satellite have been analyzed for Faraday rotation,† and the results indicate that the daytime ionosphere below 1100 km varies between 5×10^{16} and 2×10^{17} electrons/m^2. However, these data are over midlatitude during solar minimum conditions and might be expected to be somewhat lower than the results of Ross. Millman‡ has included the analysis of ionosonde data from Puerto Rico, Trinidad, and Bogota, Columbia, in a study of low-latitude electron content. The daytime values of the subpeak content appeared to be approximately 10^{17} electrons/m^2 for several days in the winter of 1961. After normalizing to zero sunspot number Yeh and Swenson§ have found that the electron content over Illinois varies between roughly 1 and 2×10^{17} electrons/m^2 during midday. Prior to normalization the values were much higher than this, e.g., 7×10^{17} electrons/m^2. These studies suggest that there is very little, if any, incompatibility between the Gemini IX results and previously determined estimates of

$$\int_0^{300} N\,dh.$$

*F.H. Hibberd and W.J. Ross, J. Geophys. Res. 71(No. 9):2243 (May 1, 1966).

†J.M. Goodman, "Ionospheric Parameters Derived From Echo II Radar Returns During Solar Minimum Conditions," NRL Report 6375, Feb. 21, 1966.

‡G.H. Millman, "The Variation of Electron Content in the Ionosphere at a Low Latitude," in "Electron Density Profiles in the Ionosphere and Exosphere," Jon Frihagen, editor, Amsterdam:North-Holland, 1966.

§K.C. Yeh, and G.W. Swenson, J. Geophys. Res. (66):1061 (Apr. 1961).

Assuming a mean molecular weight of 24* and a mean gravitational altitude of 250 km we find that

$$H_s = 0.0379\,T, \tag{5}$$

where H_s is the scale height of the distribution of electrons in kilometers and T is the ionospheric temperature in degrees Kelvin. It has been shown by Wright† that for a Chapman distribution (of the α type)

$$\tau = 4.13\,H_s, \tag{6}$$

where τ is the equivalent slab thickness of the ionosphere in kilometers. Since the ratio of the total content to the subpeak content is about 3.15 for a Chapman distribution, it follows from Eqs. (5) and (6) that

$$\tau' \approx 0.05\,T, \tag{7}$$

where τ' is the slab thickness of the subpeak ionosphere and T is its temperature. It has been noted by Bhonsle et al.‡ that, in the absence of equilibrium, T in Eq. (7) represents the average electron-ion temperature. Figure 10 shows the variation of τ' over Kauai, Hawaii, on June 4, 1966, under the assumption that

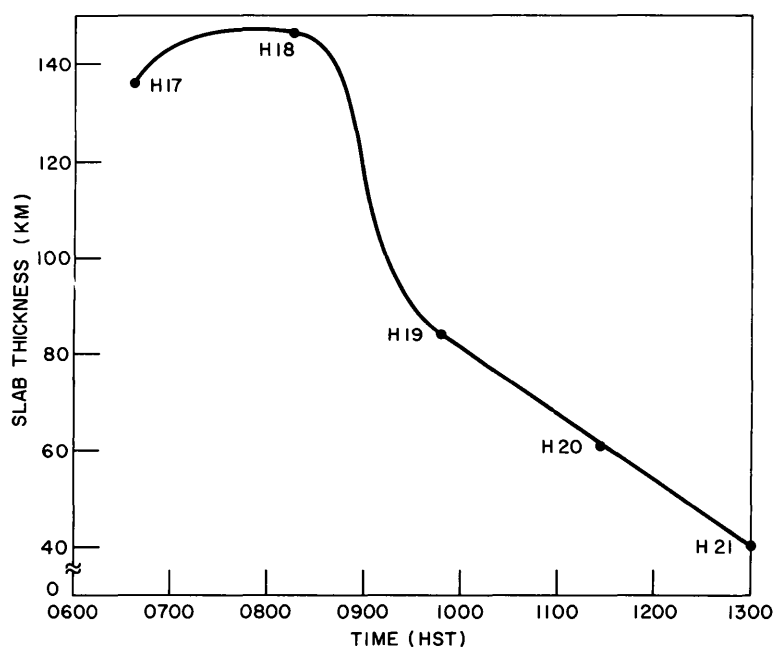

Fig. 10 - Variation of the subsatellite slab thickness τ' over Kauai, Hawaii, on June 4, 1966, where

$$\tau' = \int_{100}^{300} N\,dh/NF2$$

*The value of the molecular weight at 250 km from 1962 U.S. Std. Atmosphere. See "Handbook of Geophysics and Space Environments," S. L. Valley, editor, AFCRL, 1965.
†J.W. Wright, J. Geophys. Res. 65:185-191 (1960).
‡R.V. Bhonsle, A.V. daRosa, and O.K. Garriott, J. Res. Nat. Bur. Std., A. 69D:929 (1965).

$$\int_0^{300} N\,dh$$

essentially represents the subpeak electron content. Since the electron content

$$\int_0^{300} N\,dh$$

is not increasing at the same rate as NF2 = 1.24×10^{10} (foF2)^2, the slab thickness τ' exhibits a steady decline. The variation in τ' is probably a manifestation of the fact that the portion of the ionosphere below 200 km is closer to an equilibrium state than is that portion between 200 km and 300 km. Consequently,

$$\int_{200}^{300} N\,dh$$

increases much more rapidly than does

$$\int_0^{200} N\,dh.$$

Since the ionosphere below 300 km is neither in an equilibrium condition nor in a non-equilibrium condition, the interpretation of the slab thickness in terms of equivalent temperature is not clear. It is noteworthy, however, that the possibility of equilibrium in the subpeak ionosphere is not unlikely at midday (12 noon). Hence, the last two values of content corresponding to H20 and H21 might be useful as indicators for estimating the lower ionospheric temperature over Kauai. By inverting Eq. (7) we find that the average subpeak ionospheric temperatures were 1200°K and 800°K at 1130 HST and 1300 HST, respectively.

This, of course, has been extracted from the data under the assumption of a Chapman distribution, which requires that the ionosphere be isothermal. This is surely invalid below 300 kilometers; however, the values of T are representative of some "average" temperature — smaller than the temperature near 300 km and greater than the temperature near 100 km.

Study of the Irregularities

Since the magnetic field parameter $\bar{\psi}$ is a smoothly varying function of time, and since the Faraday rotation Ω is proportional to $\bar{\psi}$, it follows that any nonuniformities that occur in Ω as a function of time are a result of electron-content inhomogeneities.

This is, of course, subject to the proviso that the nonuniformities in Ω are real and not simply statistical fluctuations or manifestations of reading errors. Given a finite error in the measurement of Faraday rotation $\delta\Omega_e$ the smallest real percentage variation in content must be greater than the quantity 100 $\delta\Omega_e/\Omega$. Consequently, to detect a 1% variation in content in the presence of a rotation error of ±1 degree, Ω must be greater than 100 degrees. Table 2 gives the range of Ω for each transit over Hawaii and Antigua as well as the estimated rotational error $\delta\Omega_e$. Four transits — H18, H19, H21, and A18 — were considered useful for a fine-scale analysis. Figures 11 through 14 are plots of the magnetic field parameter $\bar{\psi}(t)$ for the transits under consideration, and Figs. 15 through 18 are the corresponding graphical presentations of $C(t)$. Also depicted are the errors in content δC_e corresponding to $\delta\Omega_e$. Clearly, there exist real variations in content δC which exceed δC_e, and the horizontal scales of these inhomogeneities range between 6 km and 500 km. Of the 133 irregularities detected in Gemini transits H18, H19, H21, and A18, the vast majority were between 10 km and 50 km in horizontal extent. Tables 3 through 6

Table 2
Rotational Variation for Each Transit

Transit	Range in Ω*	Average Estimated Error in Ω†
H17	$-60° < \Omega < 0°$	$\pm 0.5°$
H18	$-200° < \Omega < 90°$	$\pm 0.5°$
H19	$-160° < \Omega < 38°$	$\pm 0.5°$
H20	$-45° < \Omega < 72°$	$\pm 0.5°$
H21	$124° < \Omega < 360°$	$\pm 0.3°$
A18	$50° < \Omega < 480°$	$\pm 1.0°$

*The negative sign implies a clockwise rotation, and the absence of sign implies a counterclockwise rotation.
†Independent determinations of a particular polarization angle were in error as much as the listed value. By a comparison technique it is estimated that the sample-to-sample reading error is not appreciably greater than the absolute value of the listed error angles.

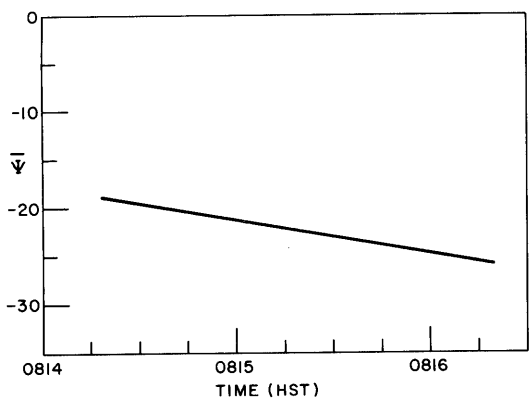

Fig. 11 - Magnetic field parameter $\bar{\psi}$ for transit H18

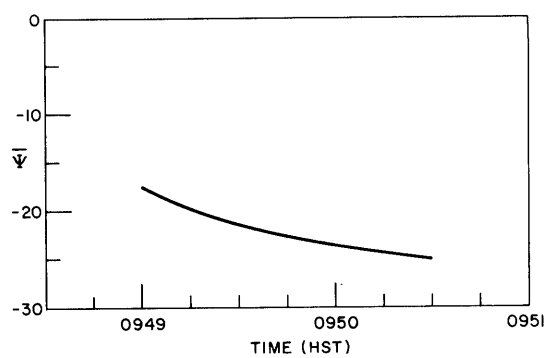

Fig. 12 - Magnetic field parameter $\bar{\psi}$ for transit H19

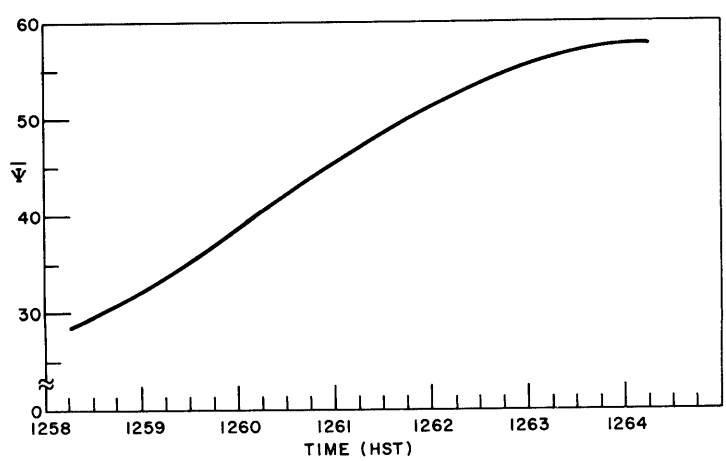

Fig. 13 - Magnetic field parameter $\bar{\psi}$ for transit H21

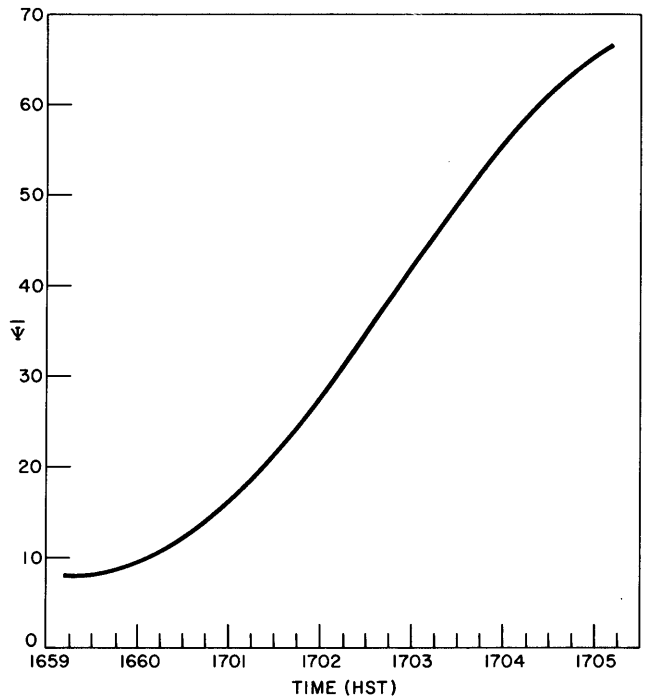

Fig. 14 - Magnetic field parameter $\bar{\psi}$ for transit A18

are listings of the observed inhomogeneities, as characterized by their mean excursions (electrons/m^2) and their scale lengths (km). Upon inspection of these tables we conclude that the true variations in content δC which occur over scales of less than 30 km are distributed uniformly. However, it is clear from the scatter diagrams (Figs. 19 through 22) that — on the average — δC is an increasing function of δL. The trend of the data suggests that there may be some linear relationship between δL and δC. Figure 23 — a composite of the data — also indicates that a quasi-linear relationship exists and is possibly common to all the data samples.

In an examination of existing ionospheric data it has been shown* that the relationship between phase excursion and horizontal scale may be approximated at 100 Mc/sec by the formula

$$\frac{\delta L}{\delta \phi} \approx 10^3 , \tag{8}$$

where δL is in meters and $\delta \phi$ is in radians. Since $\delta \phi$ is approximately 17 radians per 10^{15} electrons/m^2 at 100 Mc/sec, it follows that for all radio frequencies

$$\frac{\delta L}{\delta C} \approx 17 \times 10^{-12} , \tag{9}$$

where δC is in electrons/m^2.

*John M. Goodman, "A Note on the Polarization and Phase Characteristics of Radio Waves Propagating Through the Lower Ionosphere," NRL Report 6532, Feb. 1967.

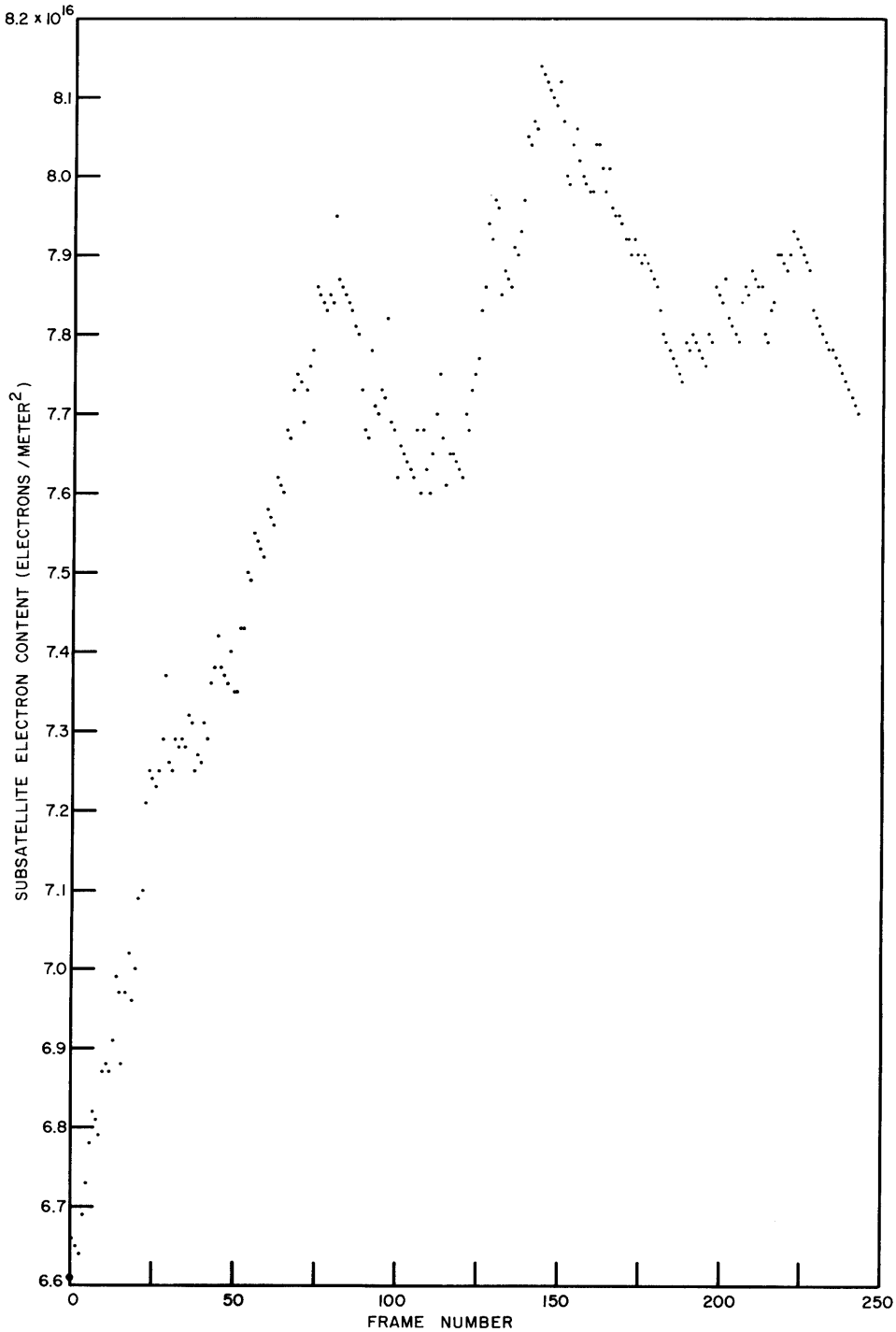

Fig. 15 - Electron content inhomogeneities associated with H18. Based upon an ionospheric mean altitude of 200 km it may be shown that $\Delta L \approx 5.14\ \Delta T$, where ΔL is in kilometers and ΔT is in seconds. Therefore, for H18 the mean frame rate of 2.02 frames/sec implies a mean ionospheric scan rate of 2.55 km/frame.

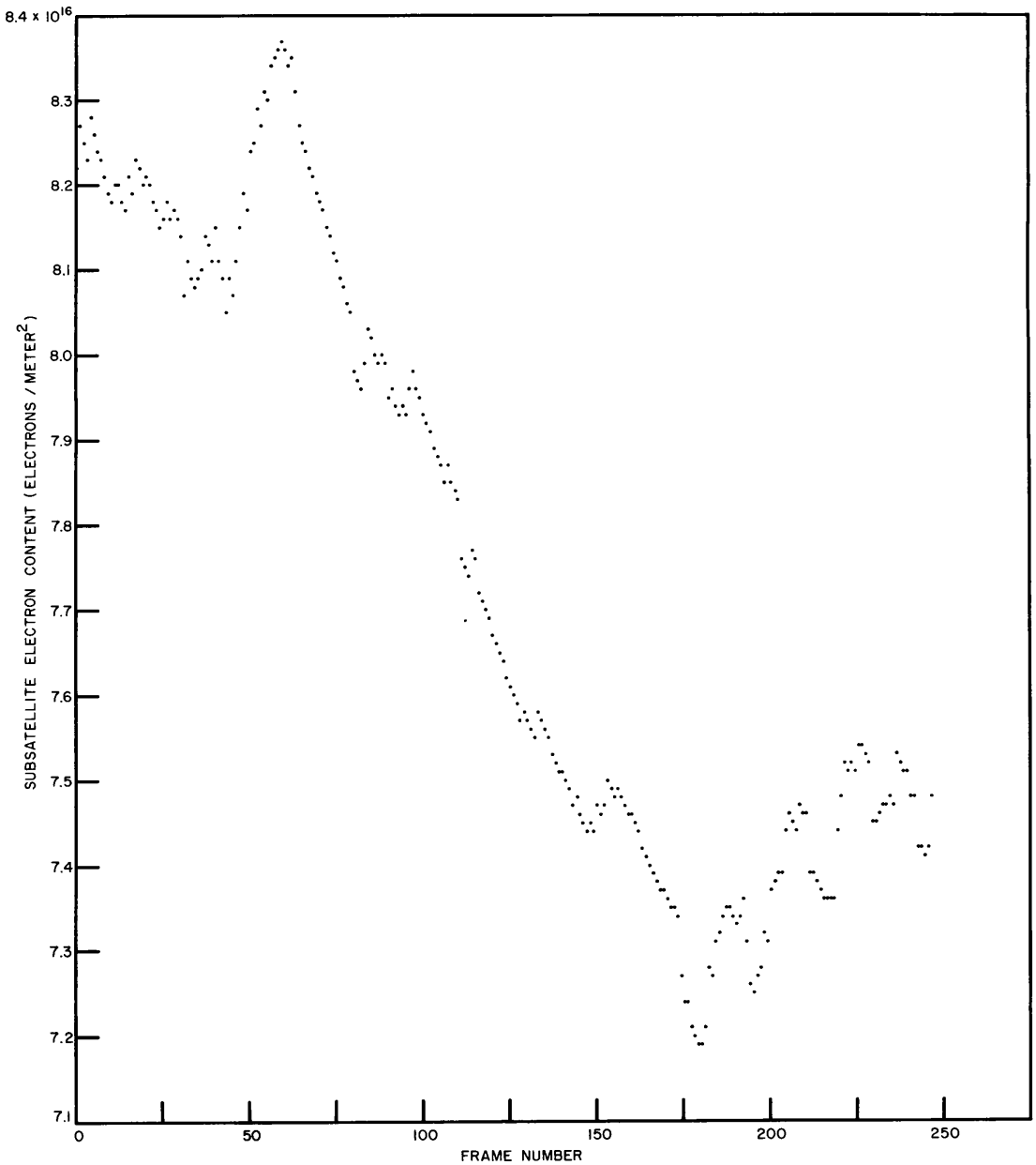

Fig. 16 - Electron content inhomogeneities associated with H19. Based upon an ionospheric mean altitude of 200 km it may be shown that $\Delta L \approx 5.14\ \Delta T$, where ΔL is in kilometers and ΔT is in seconds. Therefore, for H19 the mean frame rate of 2.50 frames/sec implies a mean ionospheric scan rate of 2.05 km/frame.

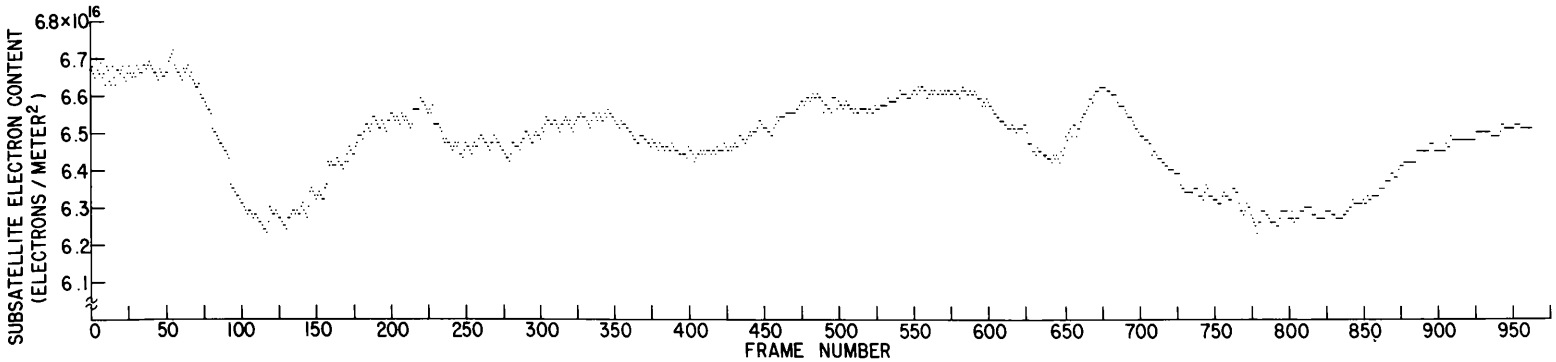

Fig. 17 - Electron content inhomogeneities associated with H21. Based upon an ionospheric mean altitude of 200 km it may be shown that $\Delta L \approx 5.14\ \Delta T$, where ΔL is in kilometers and ΔT is in seconds. Therefore, for H21 the mean frame rate of 2.92 frames/sec implies a mean ionospheric scan rate of 1.76 km/frame.

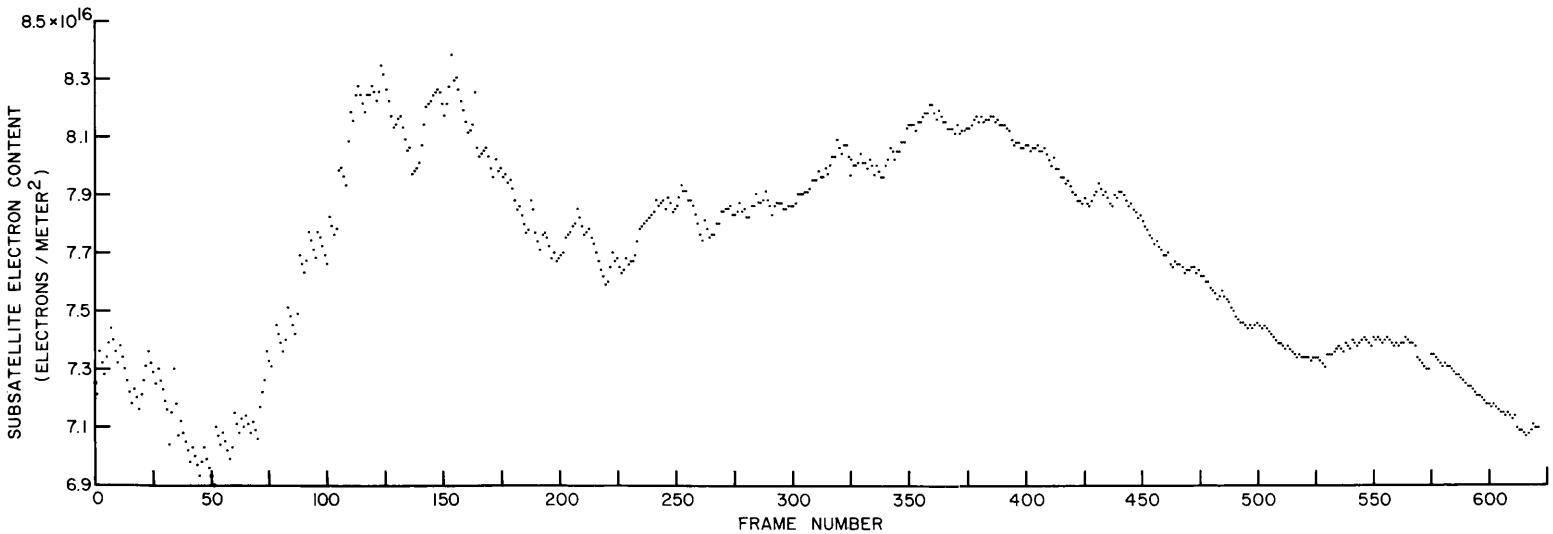

Fig. 18 - Electron content inhomogeneities associated with A18. Based upon an ionospheric mean altitude of 200 km it may be shown that $\Delta L \approx 5.14\ \Delta T$, where ΔL is in kilometers and ΔT is in seconds. Therefore, for A18 the mean frame rate of 2.08 frames/sec implies a mean ionospheric scan rate of 2.47 km/frame.

Table 3
Electron Content Inhomogeneities and Horizontal Scales Associated with H18

Irregularity* Number	δC (10^{14} electrons/m^3)	$P_{\delta c}$ (%)	δL (km)
1	11.5	1.51	10.21
2	13.0	1.70	12.76
3	16.0	2.10	22.97
4	7.0	0.92	10.21
5	12.5	1.64	10.21
6	6.5	0.85	5.10
7	8.0	1.05	7.66
8	14.5	1.90	12.76
9	20.5	2.69	25.52
10	7.5	0.98	15.31
11	6.0	0.79	10.21
12	5.0	0.66	17.86
13	9.5	1.24	25.52
14	9.0	1.18	22.97
15	42.5	5.57	158.22
16	29.5	3.86	191.39

*The order is not significant. This holds throughout the tables.

Table 4
Electron Content Inhomogeneities and Horizontal Scales Associated with H19

Irregularity Number	δC (10^{14} electrons/m^3)	$P_{\delta c}$ (%)	δL (km)
1	13.0	1.66	29.64
2	16.0	2.05	42.00
3	14.0	1.79	22.23
4	10.0	1.28	24.70
5	18.0	2.30	54.34
6	8.5	1.09	19.76
7	8.5	1.09	17.29
8	35.0	4.48	74.10

Equation (9) is represented by the straight line on Fig. 23, from which it is seen that agreement between the previous data and the Gemini IX results is reasonably good. By transforming the irregularity excursion to percentage terms we conclude from Fig. 24 that the percent excursion in content increases between 1% and 5% per 100 km. Excluding the smallest scales a median value of 2% per 100 km appears to be a reasonable fit to the data points. There is little theoretical precedent for the assumption of linearity between $P_{\delta C}$ and δL, but its designation experimentally is in agreement with the work of Bhonsle.* In his paper $P_{\delta C}$ is found to be an increasing function of δL, and a straight line has been shown to approximate the tendency of the data points. It is noteworthy that the values of $P_{\delta C}$ (%) per 100 km obtained by Bhonsle (which he denotes by $\Delta I/I$ (%) per

*R.V. Bhonsle, J. Geophys. Res. 71:4571 (1966). Bhonsle's results are based upon a differential doppler analysis of 40-Mc/sec and 360-Mc/sec radio waves from S-66. S-66 was in circular orbit at an altitude of 1000 km.

Table 5
Electron Content Inhomogeneities and Horizontal Scales Associated with H21

Irregularity Number	δC (10^{14} electrons/m^3)	$P_{\delta c}$ (%)	δL (km)
1	4.0	0.62	6.26
2	3.5	0.54	6.26
3	5.5	0.85	8.35
4	5.0	0.77	8.35
5	4.5	0.69	6.26
6	4.0	0.62	8.35
7	3.0	0.46	10.43
8	4.0	0.62	22.05
9	7.5	1.16	25.04
10	5.0	0.77	20.87
11	5.5	0.85	27.13
12	4.5	0.69	29.22
13	7.0	1.08	22.88
14	3.5	0.54	10.56
15	4.0	0.62	15.84
16	3.5	0.54	12.32
17	9.0	1.39	47.52
18	4.5	0.69	10.56
19	7.5	1.16	28.16
20	4.0	0.62	8.80
21	3.0	0.46	10.56
22	4.0	0.62	14.08
23	6.0	0.93	21.12
24	3.0	0.46	12.32
25	4.0	0.62	22.88
26	2.5	0.33	19.07
27	5.0	0.77	40.04
28	4.0	0.62	20.98
29	3.5	0.54	9.53
30	5.0	0.77	13.35
31	3.5	0.54	7.67
32	4.0	0.62	19.19
33	2.5	0.33	15.35
34	3.0	0.46	21.11
35	3.0	0.46	5.76
36	3.5	0.54	13.43
37	2.5	0.33	9.59
38	3.0	0.46	15.35
39	3.5	0.54	15.35
40	2.5	0.33	7.67
41	3.0	0.46	5.82
42	3.5	0.54	7.76
43	3.5	0.54	11.64
44	4.0	0.62	23.28
45	2.5	0.33	11.64
46	4.5	0.69	15.52
47	7.0	1.08	19.40
48	4.0	0.62	21.34
49	3.0	0.46	23.28
50	2.0	0.31	15.52
51	2.0	0.31	7.76
52	2.0	0.31	5.82
53	2.0	0.31	7.76
54	40.0	6.18	264.0
55	15.0	2.32	198.0
56	15.0	2.32	262.0
57	20.0	3.09	192.0
58	35.0	5.41	533.0

Table 6
Electron Content Inhomogeneities and Horizontal Scales Associated with A18

Irregularity Number	δC (10^{14} electrons/m^3)	$P_{\delta c}$ (%)	δL (km)
1	11.5	1.50	7.42
2	14.0	1.82	14.83
3	21.0	2.73	29.66
4	15.5	2.02	17.30
5	26.0	3.38	32.14
6	24.5	3.19	12.36
7	10.0	1.30	12.36
8	15.5	2.02	17.30
9	26.0	3.38	17.30
10	20.0	2.60	9.89
11	11.5	1.50	12.36
12	22.0	2.86	22.25
13	11.5	1.50	12.36
14	10.0	1.30	12.36
15	11.0	1.43	7.42
16	14.5	1.89	12.36
17	21.5	2.80	19.78
18	16.5	2.15	17.30
19	55.0	7.16	123.60
20	32.0	4.17	59.33
21	19.0	2.47	34.61
22	24.0	3.12	19.78
23	18.0	2.34	12.36
24	14.5	1.89	14.83
25	8.0	1.04	12.36
26	22.0	2.86	51.91
27	9.0	1.17	17.30
28	22.0	2.86	64.27
29	7.0	0.91	14.83
30	7.0	0.91	7.42
31	4.5	0.59	12.36
32	8.5	1.11	19.77
33	18.5	2.41	86.32
34	17.5	2.28	64.27
35	5.5	0.72	14.32
36	7.0	0.91	14.32
37	8.0	1.04	19.77
38	7.0	0.91	22.25
39	9.5	1.24	42.03
40	8.0	1.04	24.72
41	6.5	0.85	17.30
42	7.0	0.91	34.61
43	7.5	0.98	34.61
44	10.5	1.37	88.99
45	3.0	0.39	14.83
46	3.0	0.39	24.72
47	7.0	0.91	29.66
48	4.5	0.59	14.83
49	105.0	13.7	432.59
50	62.0	8.07	519.12
51	21.5	2.80	220.00

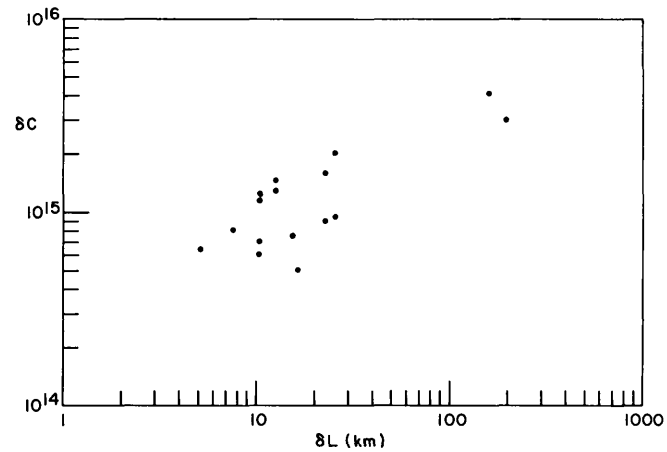

Fig. 19 - Relationship between the electron content excursion δC and the horizontal scale δL for H18

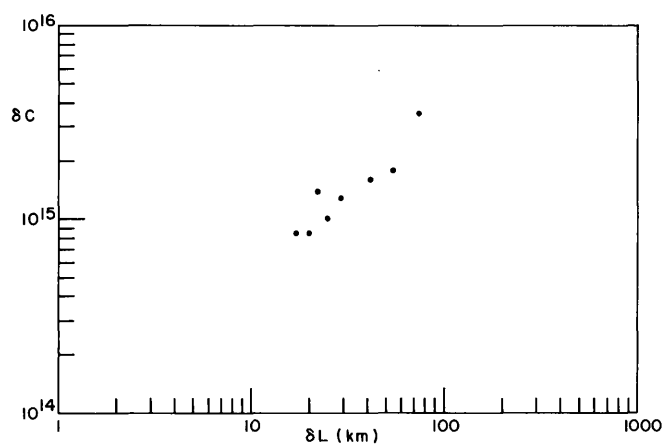

Fig. 20 - Relationship between the electron content excursion δC and the horizontal scale δL for H19

km) are referenced to one-half the irregularity. That is, he has determined the percentage excursion between adjacent extrema, whereas we have determined the mean excursion between nonadjacent extrema. Under the presumption of a quasi-symmetrical irregularity structure in the horizontal plane (roughly true in our data) we must multiply the values of $P_{\delta C}$ obtained by Bhonsle by 1/2. From Fig. 24, we see that there is quite a large discrepancy between Bhonsle's total ionospheric daytime results and the lower ionospheric results presented in this report. It is emphasized that the NRL results are based upon the lower ionosphere in the low latitudes and that Bhonsle's results are based upon the majority of the ionosphere over a middle-latitude station. The fact that larger percentage excursions are observed in the NRL results may be the manifestation of a uniform distribution (in terms of both scale and content excursion) of inhomogeneities.

Assuming that there is negligible superposition of supersatellite irregularities upon the subsatellite irregularity pattern, it follows from

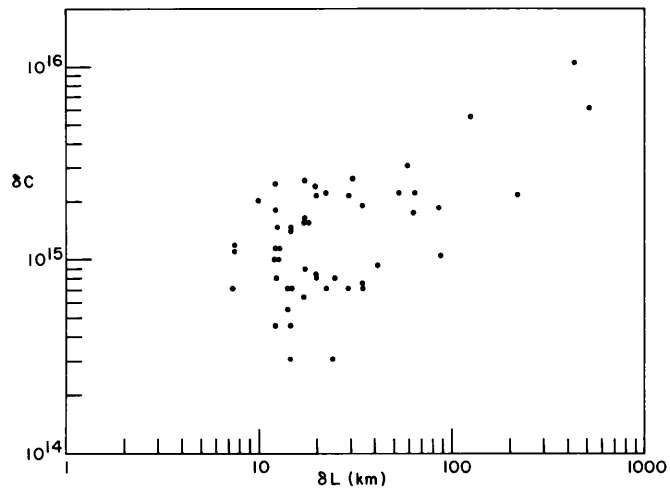

Fig. 21 - Relationship between the electron content excursion δC and the horizontal scale δL for H21

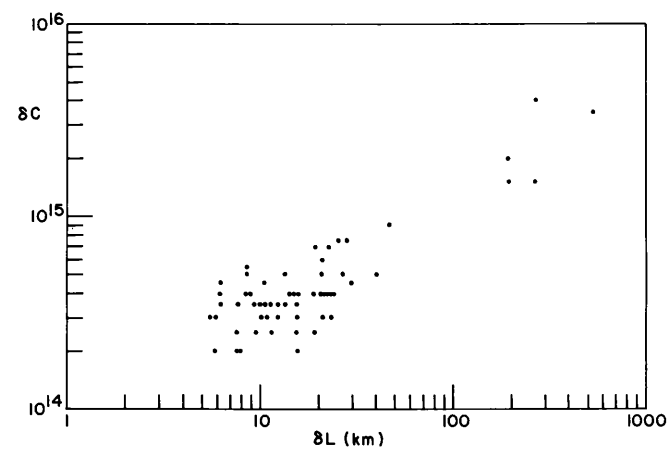

Fig. 22 - Relationship between the electron content excursion δC and the horizontal scale δL for A18

$$\int_0^{hF2} N\,dh \Big/ \int_0^{\infty} N\,dh \approx 1/3 \tag{10}$$

that $P_{\delta C}$, corresponding to the whole ionosphere, should be approximately 1/3 the value of $P_{\delta C}$, corresponding to

$$\int_0^{hF2} N\,dh.$$

For the D-14 experiment it was generally true that $hF2$ was greater than the spacecraft altitude of 300 km. Consequently, it would be anticipated that the relationship

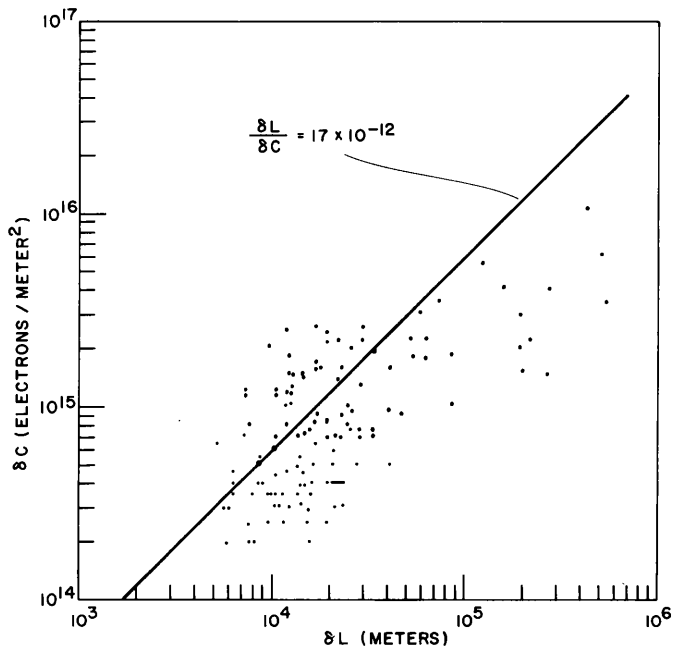

Fig. 23 - Relationship between the electron content excursion δC and δL for all transits

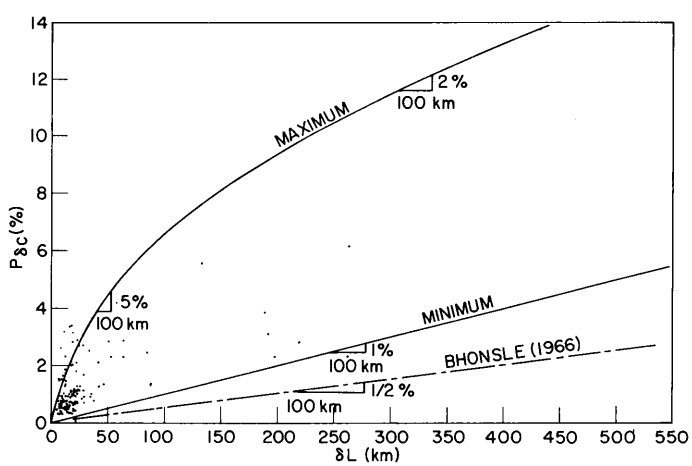

Fig. 24 - Relationship between the percentage excursions in the subsatellite electron content and their horizontal scales for H18, H19, H21, and A18

$$P_{\delta C}(h_s) \approx 3P_{\delta C}(\infty), \tag{11}$$

where ∞ implies the total content and h_s implies the subspacecraft content, would surely be true.

The enhanced excursions in $P_{\delta C}$ could also be explained by the theory of irregularity amplification,* which at F-region heights is more pronounced near the magnetic equator than near the middle latitudes.

Although it might be presumptuous to construct a composite law based upon these data, there is nevertheless sufficient practical interest in relations of the form

$$P_{\delta C} = m\delta L, \tag{12}$$

where m varies between 1% and 5% per 100 km, to warrant a few remarks. Such a relationship between $P_{\delta C}$ and δL implies that $P_{\delta C}$ and δL are one-to-one and that nonvanishing values of $P_{\delta C}$ are defined for all $\delta L > 0$ and are continuous throughout the domain of definition. To a certain extent all three implications are false. The data-point scatter in Figs. 23 and 24 suggests that $P_{\delta C}$ is neither one-to-one with δL nor continuous in the strict mathematical sense. Taking some liberty with the mathematics, however, it may be said that there is some tendency for $P_{\delta C}$ to be continuous as well as one-to-one with δL. That is, given a value of $P_{\delta C}$, say $P_{\delta C_i}$, there exists on the average a unique value of horizontal scale $(\delta L)_i$. Conversely, given a value of δL, say $(\delta L)_i$, there exists on the average a unique value of percentage excursion $P_{\delta C_i}$. An on-the-average continuity concept can be similarly argued. Of course these remarks are trivial consequences of the fact that we propose, a priori, a relationship between δC and δL which has the desired characteristics, namely, that $P_{\delta C}$ and δL are one-to-one and that $P_{\delta C}$ is a continuous function of δL.

In brief, Eq. (12) or any similar relations, must be interpreted as follows: Corresponding to a particular scale length $(\delta L)_i$ (it it exists) there is an average electron content percentage excursion $P_{\delta C_i}$ which may be derived in accordance with some rule, say Eq. (12).

Assuming that the inhomogeneities are sinusoidal with period δL and that a continuity of scales exists and recurs ad infinitum, it is easy to estimate the number of occurrences of a particular scale if the distance D over which observations are made is finite. The distribution is determined by the fraction $D/\delta L$ and is presented in Fig. 25. Of course, in reality, the actual detection of such a distribution function is subject to the coupling between the various scales as well as the content excursions they represent. Figure 26 is the scale length distribution corresponding to the four Gemini transits under consideration. The fact that fewer irregularities with scales between 0 km and 10 km appear is simply a manifestation of the sampling rate and is not felt to be a real effect. There was also a tendency to disregard certain excursions which appeared to be the result of reading errors, and these excursions were predominantly associated with the smallest scales. Let $N(\delta L)$ refer to the number of irregularities with scale length δL which may be detected within a distance D; then $N(\delta L_1)/N(\delta L_2) = \delta L_2/\delta L_1$, and the anticipated distribution function normalized to the number of occurrences between 10 km and 20 km may be computed quite readily and is included in Fig. 26. It is evident that the observed distribution of scales drops off much more rapidly than the anticipated normalized distribution. This implies that the smaller scales between 10 km and 30 km occur in much greater numbers than would be anticipated strictly on the basis of their size and the sample time.

*D.H. Schrader, and J.R. Kan, J. Geophys. Res. 71:5617 (1966).

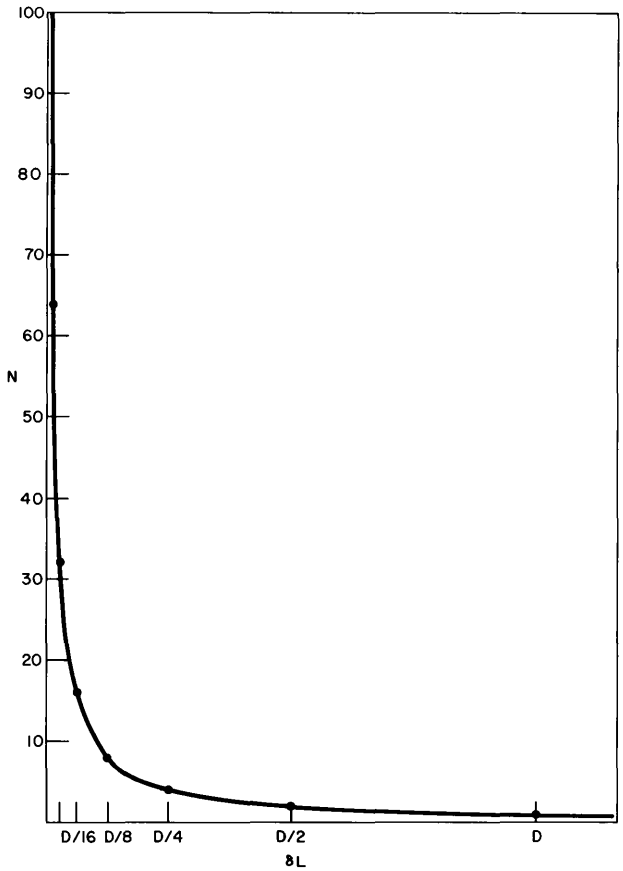

Fig. 25 - Distribution of scales δL under the assumption that the ionosphere is "filled" with all possible scales. D is the duration (in kilometers) of the sample, and N is the number of occurrences of a particular scale length δL.

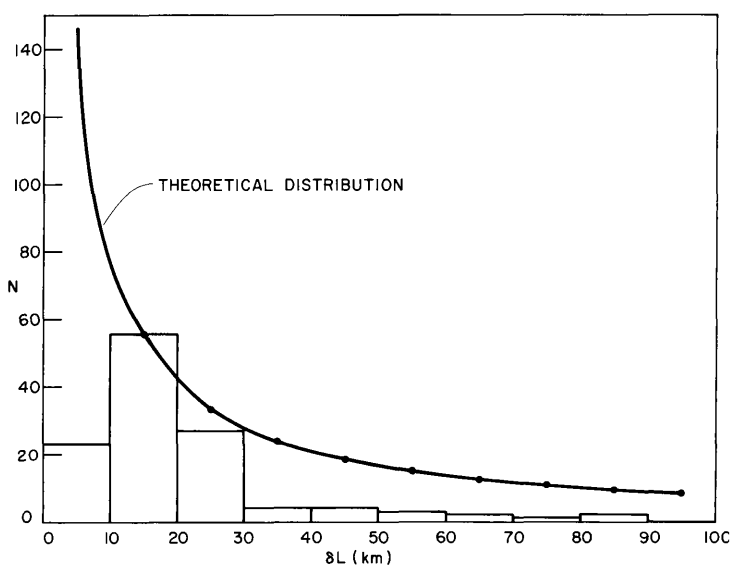

Fig. 26 - Scale length distribution corresponding to observed electron content inhomogeneities. The smooth curve is the theoretical distribution of scales normalized to the number of occurrences between 10 km and 20 km.

Since the mean free path is an increasing function of altitude (approximately 16 cm at 100 km altitude and about 30 km at 700 km altitude) it is likely that smaller-scale inhomogeneities could be produced more readily in the lower ionosphere than in the upper ionosphere. Furthermore, turbulence theory suggests that ionospheric inhomogeneities may exist only in the 200 km to 300 km altitude region.* Consequently, the data presented in this report verify the generally accepted notion that small-scale inhomogeneities are present in the lower ionosphere. Furthermore, the normalized probability of occurrence $N/N_{theoretical}$ is greater for the smaller inhomogeneities than for the larger ones.

Discussion of Errors

The possible errors associated with an experiment of this type may be divided into two classes — regular and irregular. Regular errors may result from imprecise knowledge of the magnetic field parameter $\bar{\psi}$ or some misalignment of the spacecraft antenna, and irregular errors might arise from irregular motion of the spacecraft about its own center of gravity or from scaling errors related to the film reading and data-reduction processes. Irregularities in the subsatellite electron content will produce variations in the polarization of the received signal. To properly measure these variations we require that the irregular error sources be small in comparison. Another possible source of irregular error would be a result of fine-scale nonuniformities in the earth's magnetic field.

It is difficult to state the absolute errors corresponding to some of the error sources; however, it is usually possible to estimate these errors reasonably well. For example, the regular errors in the computed values of content are proportional to the regular errors in the parameter $\bar{\psi}$. This parameter is probably accurate to better than 5%, which implies that the true values of content, on an absolute basis, are within 5% of the computed values. Since Navy Oceanographic Office charts do not exhibit fine-scale variations in the magnetic field intensity H or in the inclination or declination, it is anticipated that fine-scale variations in these quantities should not be appreciable at ionospheric heights. Consequently, no irregular variations in $\bar{\psi}$ are expected, and this implies that the magnetic field representation introduces only a regular error into the electron content analysis.

The signals fed into the x-y oscilloscope exhibited a signal-to-noise ratio of about 10 dB. A signal-to-noise ratio of this magnitude implies a 20% random error approximately 50% of the time, and the maximum angular error corresponding to a 20% random error is about 10 degrees. An error of this magnitude would certainly render all the fine-scale data analysis meaningless, since, generally, the "ionospheric component" of the irregular polarization changes are typically a few degrees. Fortunately, however, enough traces of the polarization "ellipse"† were superimposed on the oscilloscope screen during the film exposure time to render a considerable integration of the random noise. In fact, the scope presentation frequency of 120 kc/sec and the exposure time of 2/10 sec implies that 24,000 ellipses are superimposed on each frame-by-frame picture of the oscilloscope screen. This amount of superposition reduces the random error problem to a reading error problem, which may be estimated quite easily. Due to the resultant "thickness" of the presentation there is some ambiguity concerning the exact placement of the semimajor axis of the ellipse. However, by comparing readings of the polarization corresponding to a given frame obtained by independent observations, it was

*H.G. Booker, "Polar Atmosphere Symposium," New York: Pergamon Press, p. 52, 1957.
†An ellipse in the mathematical sense is not prescribed in general. However, the effect of random noise and extraneous phase errors is to open the straight line which should theoretically appear. This opening of the line is produced by a change in the relative phase between the x and y channels over a time period of approximately 10 μsec.

found that the error was usually equal to or less than 1/2 degree. The tabulation of the estimated reading error is included in Table 2.

During the time the D-14 experiment was conducted the spacecraft computer controlled the spacecraft position. Consequently, no antenna misalignment errors, and negligible irregular errors, were introduced. The precision of the platform orientation, as defined by roll, pitch, and yaw, is estimated to be about 1/100 degree. The reading error of 1/2 degree obviously dominates the systematic errors introduced by the irregular variations of the spacecraft attitude.

CONCLUSIONS

Vhf radio transmissions from the spacecraft Gemini IX have been analyzed for irregular variations in polarization. The additional use of the uhf radio transmission was the primary factor in the successful removal of the vhf Faraday rotational ambiguity; but, as expected, it was not very useful for fine-scale polarization studies.

A Faraday rotation study using a frequency of 133 Mc/sec is not sufficiently accurate within about 10° of the transverse condition, since the amount of rotation in that region is small and the relative error is inversely proportional to the total rotation.

Furthermore, the quasi-longitudinal approximation is not valid for propagation angles which are within 2° of being transverse at 133 Mc/sec. Four of the analyzed transits exhibit a quasi-transverse condition, but it is not persistent for any transit.

The subsatellite electron content varied between 5×10^{16} and 8×10^{16} electrons/m^2 over Kauai, Hawaii, between 0700 and 1300 local time. Over Antigua the content was roughly 8×10^{16} electrons/m^2 at midday.

Ionosonde data from nearby Maui, Hawaii, was useful in computing the effective slab thickness of the subsatellite ionosphere. It was found to be a decreasing function of time and its minimum value was obtained at midday. The measured diurnal range in effective slab thickness below 300 km was 40 km to 140 km. Taking 50 km to be an equilibrium value of slab thickness, it was determined that the lower ionospheric mean temperature was approximately 1000°K at midday.

A decrease in subsatellite content between transits H20 and H21 suggests the existence of strong vertical drift forces in the low-latitude ionosphere. However, this is a tentative suggestion based upon a small sample of data.

The magnitudes and horizontal scales of ionospheric inhomogeneities below 300 km were determined. The relationship between percent excursion in content $P_{\delta c}$ and horizontal scale δL in kilometers may be approximated by

$$P_{\delta c} \cong m\,\delta L\,, \tag{13}$$

where m is a slope factor which ranges between 1% and 5% per 100 kilometers. This slope is somewhat larger than previous estimates based upon the total ionospheric path.

ACKNOWLEDGMENTS

The authors acknowledge the contributions made to this project by Mr. L. L. Gasch and Mr. W. L. Thrift by their dedicated and untiring efforts in the installation and operation of the two ground receiving stations. The authors also acknowledge the efforts of Mr. O. F. Borchardt, Mr. J. R. Brinson, and Mr. W. E. Gillette in operating the ground receiving stations during the experiments.

APPENDIX

DERIVATION OF THE FARADAY EFFECT FOR A COLLISION-FREE ANISOTROPIC PLASMA

In a magneto-ionic medium the two characteristic wave refractive indices are defined by the Appleton-Hartree formula*

$$n^2 = 1 - \frac{X}{1 - iZ - Y_T^2/2(1 - X - iZ) \pm \left[Y_T^4/4(1 - X - iZ)^2 + Y_L^2\right]^{1/2}}, \tag{A1}$$

where

$X = Ne^2/\epsilon_0 m\omega^2 = (\omega_p/\omega^2)$,

$Y_L = eB_L/m\omega = (\omega_g/\omega)\cos\theta$,

$Y_T = eB_T/m\omega = (\omega_g/\omega)\sin\theta$,

ν = angular electron collision frequency,

$Z = \nu/\omega$,

N = number density of free electrons,

e = electronic charge,

ϵ_0 = free-space permittivity,

m = electronic mass,

$\omega = 2\pi f$ = radio wave angular frequency,

B = magnetic induction,

$B_L = B\cos\theta$ = longitudinal component of magnetic induction,

$B_T = B\sin\theta$ = transverse component of magnetic induction,

$\omega_g = 2\pi f_g = eB/m$ = angular electron gyrofrequency,

$\omega_p = 2\pi f_p = (Ne^2/\epsilon_0 m)^{1/2}$ = angular plasma frequency, and

θ = angle between the radiowave normal and the magnetic field vector.

Clearly, a magneto-ionic medium such as the earth's ionosphere is anisotropic, since the two characteristic wave refractive indices defined by Eq. (A1) depend upon the

*K. Davies, Nat. Bur. Stds., "Ionospheric Radio Propagation," Monograph 80, 1965.

direction of propagation. The two characteristic waves are elliptically polarized with opposite senses of rotation, and they travel with slightly different phase velocities. These waves are often referred to as the ordinary and the extraordinary waves. Since the electron collision frequency is exceedingly small in comparison with the radio frequency at vhf, the absorption parameter Z may be neglected and we have

$$n^2 = 1 - \frac{X}{1 - Y_T^2/2(1 - X) \pm \left[Y_T^4/4(1 - X)^2 + Y_L\right]^{1/2}}, \tag{A2}$$

which is critically dependent upon the angle θ. When $\theta = 90°$ we have transverse propagation, and when $\theta = 0°$ we have longitudinal propagation. The most useful relations for Faraday rotation studies arise upon consideration of the so-called quasi-longitudinal (QL) mode of propagation. The criterion for QL propagation is obtained upon examination of Eq. (A2) and may be written as

$$Y_T^4/4(1 - X)^2 << Y_L \tag{A3}$$

and

$$\frac{(\omega_g/\omega)^4 \sin^4\theta}{4\left[1 - (\omega_p/\omega)^2\right]^2} << (\omega_g/\omega)^2 \cos^2\theta. \tag{A4}$$

Inserting f_p = 10 Mc/sec, f_g = 1 Mc/sec, and f = 100 Mc/sec into Eq. (A4) and carrying out the arithmetic, one finds that QL propagation prevails over approximately all θ. The constraint defined by Eq. (A4) breaks down when the wave normal (propagation path) and the magnetic field vector are within 2° of being orthogonal. Assuming a QL mode defined by Eq. (A3) the indices of refraction may be written as

$$n^2 = 1 - X(1 \pm Y_L)^{-1} \tag{A5}$$

or

$$n^2 \cong 1 - X(1 \mp Y_L), \tag{A6}$$

since $Y_L = (\omega_g/\omega)\cos\theta << 1$ at vhf. A binomial expansion of Eq. (A6) leads to the following expressions for the ordinary and extraordinary components of the index of refraction:

$$n_1 = 1 - 1/2\, X(1 - Y_L) + \ldots, \tag{A7a}$$

and

$$n_2 = 1 - 1/2\, X(1 + Y_L) + \ldots, \tag{A7b}$$

where higher-order terms are vanishingly small for f > 100 Mc/sec. (It is clear that if B were to vanish both indices of refraction would be identical, and $n = n_1 = n_2$ would describe the refractive index for an isotropic plasma. If N were to approach zero, then, regardless of B, we see that $n = n_1 = n_2$ would approach the free-space value of unity.) Under QL propagation conditions the two characteristic waves become approximately circularly polarized; since n_1 and n_2 are both less than unity, it follows that the associated phase velocities are greater than the free-space velocity of light, but the extraordinary wave has a slightly greater velocity than does the ordinary wave.

After traversing a distance ds in a magneto-ionic medium the magnitudes of the angles formed by the electric vectors of the two characteristic waves are given by

$$d\varphi_i = (\omega/2c)\, n_i \, ds\,, \quad i = 1, 2, \tag{A8}$$

where φ_1 refers to the ordinary wave and is measured in the clockwise sense, and φ_2 refers to the extraordinary wave and is measured in the counterclockwise sense. For radio frequencies in excess of 100 Mc/sec the angle between the direction of phase propagation (wave normal) and the direction of energy propagation (ray direction) is negligibly small. As a consequence we may neglect the distinction between the directions of phase and energy propagation. In addition, the ordinary and extraordinary waves may be expected to propagate over identical paths. Assuming an equal amplitude for the two waves, it is seen that the resultant electric vector has rotated by an amount $d\phi$, over the distance ds, which is given by

$$d\phi = d\varphi_1/2 - d\varphi_2/2 = (\omega_g/2c)(\omega_p/\omega)^2 \cos\theta \, ds. \tag{A9}$$

In mks units, the differential (Faraday) rotation is given by

$$d\phi = 2.97 \times 10^{-2} f^{-2} N H \cos\theta \, ds\,, \tag{A10}$$

where $H = B/\mu_0$ is the magnetic field intensity, assuming free-space magnetic conditions.

Upon integration of Eq. (A10) over a distance S we may obtain the total Faraday rotation angle (see Fig. A1)

$$\Omega = d\phi = 2.97 \times 10^{-2} f^{-2} \int_0^S H \cos\theta \, N \, ds\,, \tag{A11}$$

where H, θ, and N are known functions of distance along the path of propagation, denoted by Γ. (For a superionospheric satellite radiating linearly polarized radio waves toward earth, one sometimes refers to the upper limit of Eq. (A11) by the symbol ∞.) Surely, $\int H \cos\theta \, N \, ds \neq 0$ for the case of quasi-longitudinal propagation. However, Millman* has shown that a nonvanishing amount of rotation may exist in the transverse region. This rotation amounts to about 1% of the maximum longitudinal rotation. To relate Ω to a vertical electron density distribution one uses the relation (see Fig. A2)

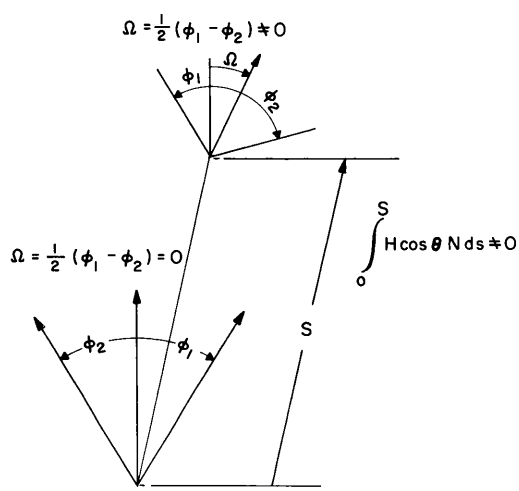

Fig. A1 - Relationship between the polarization rotation Ω and the phase difference between the two magneto-ionic components ϕ_1 and ϕ_2

*G.H. Millman, "A Survey of Tropospheric, Ionospheric, and Extraterrestrial Effects on Radio Propagation Between the Earth and Space Vehicles," General Electric Report TIS R66EMH1, Jan. 1966.

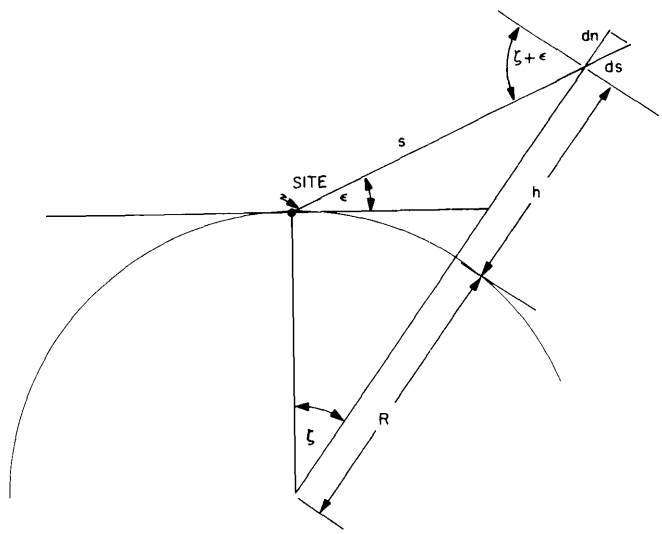

Fig. A2 - Ray path geometry

$$ds = dh \sec \chi, \tag{A12}$$

where χ is the local zenith angle and dh is the differential altitude. Substituting $dh \sec \chi$ for ds in Eq. (A11) one obtains

$$\Omega = 2.97 \times 10^{-2} f^{-2} \int_0^{h_s} H \cos \theta \sec \chi \, N \, dh, \tag{A13}$$

where h_s is the altitude corresponding to the upper limit in Eq. (A11).

This substitution enables one to discuss vertical electron density functions and is an obvious convenience for comparing results obtained over a variety of values of χ. It must be remembered, however, that any vertical density function $N(h,\Gamma)$ is also a function of the radio path Γ. In the limit of spherical stratification $N(h)$ is independent of Γ. If one denotes $H \cos \theta \sec \chi$ by ψ, Eq. (A13) becomes

$$\Omega = 2.97 \times 10^{-2} f^{-2} \int_0^{h_s} \psi \, N \, dh \, . \tag{A14}$$

Along each path of wave propagation Γ, ψ is a continuous function of the measured distance s on Γ; consequently, from Eq. (A12), ψ is a continuous function of altitude h. Since $N(h)$ is everywhere positive and ψ is continuous, one may apply the theorem of the mean to Eq. (A14), provided $N(h)$ is also continuous, and obtain

$$\Omega = 2.97 \times 10^{-2} f^{-2} \bar{\psi} \int_0^{h_s} N \, dh \, , \tag{A15}$$

where

$$\bar{\psi} = \frac{\int_0^{h_s} \psi \, N \, dh}{\int_0^{h_s} N \, dh}$$

and is called the magnetic field parameter. Equation (A15) expresses the Faraday rotation as proportional to the product of $\bar{\psi}$ and the electron content and inversely proportional to the square of the radio frequency. This implies that

$$\int_0^{h_s} N \, dh$$

is readily obtainable, provided Ω may be measured unambiguously.

This page intentionally left blank.

Security Classification

DOCUMENT CONTROL DATA - R & D

(Security classification of title, body of abstract and indexing annotation must be entered when the overall report is classified)

1. ORIGINATING ACTIVITY *(Corporate author)*
Naval Research Laboratory
Washington, D.C. 20390

2a. REPORT SECURITY CLASSIFICATION
Unclassified

2b. GROUP

3. REPORT TITLE
FINAL REPORT ON GEMINI EXPERIMENT D-14 UHF-VHF POLARIZATION MEASUREMENTS

4. DESCRIPTIVE NOTES *(Type of report and inclusive dates)*
A final report on the problem.

5. AUTHOR(S) *(First name, middle initial, last name)*
R.E. Ellis, J.M. Goodman, and W. Sievers

6. REPORT DATE
October 20, 1967

7a. TOTAL NO. OF PAGES
40

7b. NO. OF REFS
17

8a. CONTRACT OR GRANT NO.
NRL Problem R07-13

b. PROJECT NO.
A37-538-006/6521/F019-02-01

c.

d.

9a. ORIGINATOR'S REPORT NUMBER(S)
NRL Report 6591

9b. OTHER REPORT NO(S) *(Any other numbers that may be assigned this report)*

10. DISTRIBUTION STATEMENT
This document has been approved for public release and sale; its distribution is unlimited.

11. SUPPLEMENTARY NOTES

12. SPONSORING MILITARY ACTIVITY
Department of the Navy (Naval Air Systems Command – Astronautics Division, Washington, D.C. 20360

13. ABSTRACT

A vhf-uhf Faraday rotation experiment (D-14) was conducted in conjunction with six Gemini IX spacecraft transits over Kauai, Hawaii, and Antigua, British West Indies, on June 4, 1966. The rotational ambiguity at vhf was resolved by inspecting the received uhf polarization. The electron content and its inhomogeneities below the spacecraft have been determined. By comparing the results of the data analysis corresponding to four closely spaced transits of Gemini IX over Hawaii, a measure of the prenoon electron-content variation was obtained. Assuming a Chapman distribution and equilibrium conditions, the lower ionospheric temperature has been estimated to be approximately 1000°K at midday.

It has been found that the smaller ionospheric inhomogeneities (approximately 10 to 30 km) occur in greater numbers than would be anticipated strictly on the basis of their size and sample-time considerations. The irregularity excursion δC is found to be roughly an increasing function of irregularity scale δL, with the percentage excursion $P_{\delta c}$ increasing between 1% and 5% per 100 km.

DD FORM 1 NOV 65 1473 (PAGE 1)

S/N 0101-807-6801

Security Classification

Security Classification

14. KEY WORDS	LINK A ROLE	LINK A WT	LINK B ROLE	LINK B WT	LINK C ROLE	LINK C WT
Polarization measurement [uhf-vhf]						
Ionosphere						
Electron content						
Inhomogeneities						
Electron distribution						
Ambiguity removal						
Faraday effect						

DD FORM 1 NOV 65 1473 (BACK) (PAGE 2) GPO 931-710

Security Classification